Aus dem
Lehrstuhl für Physiologische Genomik,
Biomedizinisches Centrum (BMC)
Institut der Ludwig-Maximilians-Universität München

Muscle Spindle Structure in a Mouse Model for Pompe Disease

Dissertation

zum Erwerb des Doktorgrades der Medizin

an der Medizinischen Fakultät

der Ludwig-Maximilians-Universität München

vorgelegt von

Andi Rafuna

aus

Prishtina

Jahr

2025

Mit Genehmigung der Medizinischen Fakultät der

Ludwig-Maximilians-Universität zu München

Erster Gutachter:	Prof. Dr. Stephan Kröger
Zweiter Gutachter:	Prof. Dr. Benedikt Schoser
Dritter Gutachter:	Prof. Dr. Eric Hesse
Mitbetreuung durch den promovierten Mitarbeiter:	Prof. Dr. Anja Horn Bochtler
Dekan:	Prof. Dr. med. Thomas Gudermann
Tag der mündlichen Prüfung:	18.02.2025

Table of content

Zusammenfassung

Morbus Pompe (Glykogenose Typ II) ist eine seltene, autosomal rezessiv vererbte lysosomale Glykogenspeicherkrankheit, die vor allem die Skelettmuskulatur, das Herz und das Nervensystem betrifft. Die Ursache der Morbus Pompe sind Mutationen im *Gaa* Gen, das für das Enzym Saure Maltase kodiert, welches für den Abbau von Glykogen in den Lysosomen verantwortlich ist. Das Fehlen des Enzyms führt zu einer Vergrößerung und Zerstörung der Lysosomen in allen Geweben, am stärksten jedoch in den Skelettmuskeln, was zu einer Myopathie führt. Ein weiterer Mechanismus zur Erklärung der Pompe-Krankheit ist eine Störung der Autophagie.

Patienten mit Morbus Pompe haben neben einer fortschreitenden und generalisierten Muskelschwäche eine geringere Gang- und Standstabilität, was zu einem erhöhten Risiko für Stürze und zu Krankenhausaufenthalten führt. Frühere Studien haben gezeigt, dass diese Instabilität nur teilweise durch die Myopathie erklärt werden kann. Eine alternative Ursache könnte sein, dass Patienten mit Morbus Pompe eine gestörte Propriozeption haben. Um dieser Hypothese nachzugehen, habe ich die Morphologie der Muskelspindeln (die Hauptpropriozeptoren) von 2.5 und 8.5 Monate alten Mäusen mit einer genetischen Defizienz von Saurer Maltase ($Gaa^{-/-}$ Mäuse) qualitativ und quantitativ untersucht, und zwar im vorwiegend „slow-twitch“ Soleus Muskel und im vorwiegend „fast-twitch“ Extensor Digitorum Longus Muskel. In den 2.5 Monate alten $Gaa^{-/-}$ Mäusen zeigte die Morphologie der Muskelspindel keine signifikanten Veränderungen, es waren nur einige autophagische Vakuolen vorhanden. Die quantitative Analyse zeigte jedoch, dass die umlaufenden Elemente der sensorischen Nervenendigungen breiter und kürzer waren, was durch Einlagerung von Glykogen oder autophagischen Aufbau verursacht werden könnte. In 8.5 Monate alten $Gaa^{-/-}$ Mäusen wiesen die Muskelspindeln eine schwere Degeneration auf, einschließlich des vollständigen Fehlens der sensorischen Nervenenden, einer Auflösung der intrafusalen Fasern und einem erheblichen autophagischen Rückstau. Außerdem ergab die Quantifizierung der Anzahl der Muskelspindeln im M. soleus der 8.5 Monate alten Gaa^{-}

/- Mäuse eine verringerte Anzahl, was auf die starke Degeneration der Muskelspindeln zurückzuführen sein könnte. Diese degenerativen Veränderungen traten sowohl im vorwiegend „slow-twitch“ Soleus Muskel als auch im vorwiegend „fast-twitch“ Extensor Digitorum Longus Muskel auf. Die Degeneration der Muskelspindeln scheint also nicht von der Zusammensetzung der Muskelfaserntypen abhängig zu sein. Diese Befunde deuten darauf hin, dass die Degeneration der Muskelspindeln und die daraus resultierenden propriozeptiven Defizite die Ursache für die Gang- und Standinstabilität sowie für die häufigen Stürze bei Patienten mit Morbus Pompe sein könnten.

Abstract

Pompe disease (glycogen storage disease type II) is a rare autosomal recessive lysosomal and glycogen storage disorder, which predominantly affects the skeletal muscle, heart, and nervous system. The cause of Pompe disease are mutations in the *Gaa* gene encoding for the enzyme acid alpha-glucosidase (GAA), responsible for breaking down glycogen within lysosomes. Lack of the enzyme leads to enlargement and destruction of lysosomes in all tissues but most severely in skeletal muscle causing a myopathy. This explanation was considered incomplete, and another emerging mechanism for explaining Pompe disease is a disruption of the autophagic pathway. Patients with Pompe disease in addition to a progressive and generalized muscle weakness have gait and posture instability, resulting in an increased risk for falling and hospitalization. Previous studies have shown that this instability could only be partly explained by the myopathy. However, an additional reason could be that patients with Pompe disease have an altered proprioception. To address this hypothesis, I investigated the morphology of muscle spindles (the main proprioceptors) of 2.5- and 8.5-month-old *Gaa*$^{-/-}$ mice qualitatively and quantitatively, in the predominantly slow twitch soleus muscle and predominantly fast twitch extensor digitorum longus muscle. In 2.5-month-old *Gaa*$^{-/-}$ mice the muscle spindle morphology was not significantly altered compared to wildtype mice, showing only some small autophagic vacuoles. However quantitative analysis demonstrated that the circumferential elements of the sensory nerve terminals had a greater width and were shorter in length, which might be caused by glycogen storage or autophagic build-up. In the 8.5-month-old *Gaa*$^{-/-}$ mice the muscle spindles showed severe signs of degeneration, including a lack of sensory nerve terminals, disruption of intrafusal fibers, and considerable autophagic buildup. In addition, quantification of the number of muscle spindles in the soleus muscle of the 8.5-month-old *Gaa*$^{-/-}$ mice, showed a reduced number, which could be caused by the final degeneration of muscle spindles. These degenerative changes occurred in both the predominantly fast-twitch extensor digitorum longus muscle and the predominantly slow-twitch soleus mus-

cle. Therefore, the degeneration of the muscle spindles did not appear to be dependent on the muscle fiber type composition. These findings suggest that the degeneration of the muscle spindles and the resulting proprioceptive deficits may contribute to the gait and posture instability, as well as the frequent falls in patients with Pompe disease.

1. Introduction

Proprioception is the sense that provides the brain with information from our own musculoskeletal system (Sherrington, 1907; Kröger, 2018). The brain requires proprioceptive information, i.e., information about the length, length changes, contractile state of each muscle, muscle force, for the control of any coordinated movement, including posture and locomotion. Additionally, proprioception plays a crucial role in the effective realignment of fractured bones and in maintaining proper spinal alignment (Blecher et al., 2017, 2017). Central processing of this information allows us to precisely determine the position and movement of our extremities in space and to adjust the muscle tone to maintain a stable gait and posture (Dietz, 2002; Kiehn, 2016). The primary proprioceptive sensors are the muscle spindles. In addition to the muscle spindles, the Golgi tendon organs and joint receptors also function as proprioceptors for the musculoskeletal system (Matthews, 2015).

1.1 Muscle spindle structure

Muscle spindles are encapsulated sensory receptors and inform the brain about muscle length and the speed of muscle stretching (Proske & Gandevia, 2012). A muscle spindle of an adult mouse, measures 200-400 µm in length and consists of 3-5 encapsulated and innervated intrafusal muscle fibers that run in parallel with the extrafusal fibers (Lionikas et al., 2013; Kröger, 2018; Kröger & Watkins, 2021). In contrast to extrafusal fibers, intrafusal fibers are smaller in diameter and do not generate significant force. Based on their functional properties, the arrangement of the cell nuclei and their morphology, it is possible to distinguish between two different types of intrafusal fibers: nuclear bag and nuclear chain fibers. In nuclear bag fibers, the nuclei are clustered together, whereas in nuclear chain fibers the nuclei form a chain structure. The nuclear chain fibers are completely enclosed within the capsule and have a diameter of 10-12µm. On the other hand, nuclear bag fibers are larger in size, extend outside the capsule and have a diameter of 20-25µm. The nuclear bag fibers can be further classified into two

types known as bag1 and bag2 fibers, which are distinguished based on the specificity of their myosin ATPase (Banks et al., 1977). The nuclear bag1 fibers with their sensory afferents are most sensitive to the velocity of changes in the length of a muscle fiber, compared to the nuclear chain fibers and nuclear bag2 fibers with their sensory afferents, which are most sensitive to the amount of stretch (Boyd et al., 1977). The contractile filaments in the intrafusal fibers are restricted to the polar ends of the intrafusal fiber.

1.2 Muscle spindle innervation

Muscle spindles have both afferent (sensory) and efferent (motor) innervation. The central part of the intrafusal muscle fiber is innervated by two kinds of afferent proprioceptive sensory neurons referred to as primary or “group Ia afferents” and secondary or “group II afferents”, which are categorized based on their axonal conduction velocity (Banks, 2015; Kröger & Watkins, 2021). Type Ia afferents are myelinated, have a conduction velocity of 50–80 m/s and form the so-called annulospiral sensory endings in the center of the intrafusal fiber (Banks, 1986). Usually, there is only a single group Ia afferent neuron per muscle spindle, which innervates all of the bag1, bag2 and chain fibers within that spindle (Banks et al., 1982). Group II afferents are also myelinated, have a slower conduction velocity of 30–70 m/s and flank the primary Group I endings (Schröder et al., 1989). There are usually several of these endings and they innervate only the bag2 and chain fibers forming the so-called “flower spray” endings in the cat muscle spindle (Ruffini, 1898; Barker, 1948; Banks et al., 1982). Muscle spindles serve as stretch detectors, being able to detect the extent and rate at which a muscle is being stretched. Accordingly, action potentials are generated by afferent neurons at frequencies that are proportional to the changes in length and stretching velocity. (Matthews, 1974; De-Doncker et al., 2003). Sensory neurons that innervate bag1 fibers are most affected by the velocity of changes in muscle fiber length (dynamic sensitivity) and sensory neurons that innervate bag2 fibers or nuclear chain fibers are most affected by the amount of stretch (static sensitivity). The cell bodies of these pseudo-unipolar sensory neurons are localized in the dorsal root ganglia

(DRG) and represent just a small percentage (6–10%) of the total number of neurons in the DRG (Oliver et al., 2020).

The labeling of proprioceptive neurons can be achieved through the use of antibodies selectively targeting the vesicular glutamate transporter 1 (Honda, 1995; Wu et al., 2004). The annulospiral endings serve as the primary structures for sensing stretch, and within the spinal cord, the axons of these proprioceptive neurons establish excitatory monosynaptic connections with the corresponding α-motoneurons. These α-motoneurons then send action potentials to the homonymous target muscle (Mears & Frank, 1997; Wang et al., 2012). In addition, intrafusal muscle fibers also receive innervation from efferent γ- motoneurons, the so-called fusimotor innervation (Banks, 1994). Alpha-motoneurons are much more abundant and better characterized compared to γ-motoneurons (Manuel & Zytnicki, 2011). The γ- motoneurons make up about 30% of all the motoneurons in the ventral horn of the spinal cord. It is possible to differentiate them from α -motoneurons based on their smaller size and by several antibodies (Manuel & Zytnicki, 2011; Zhang, 2014). The axons from γ-motoneurons enter the spindle alongside the sensory axons in the equatorial region of the spindle. However, they exclusively connect with intrafusal muscle fibers at the polar ends, where they establish a cholinergic synapse. This synapse is structurally distinct but shares functional and developmental similarities with the myoneural junction formed by α-motoneurons on extrafusal muscle fibers. Gamma-motoneurons modulate the muscle spindles sensitivity by inducing contractions in the polar regions of the spindle, which leads to tension on the equatorial region of the muscle spindle (Banks, 1994; Proske, 1997). This mechanism allows for the ongoing regulation of the mechanical sensitivity of muscle spindles across the diverse range of lengths and speeds encountered during typical motor activities.

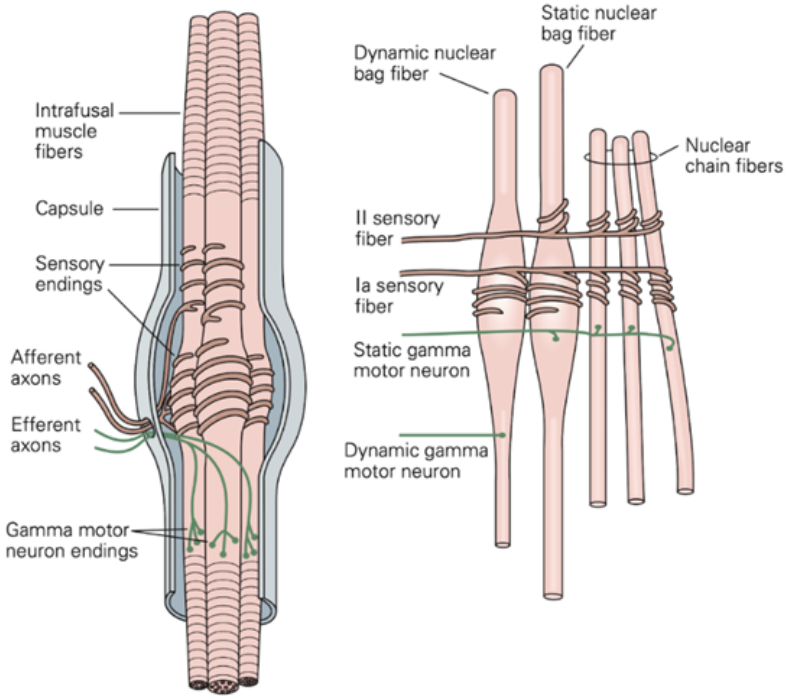

Figure 1. Schematic Representation of Muscle Spindle Structure and Innervation. (Source: Principles of Neural Science, Fifth Edition, Kandel et al., 2012). The muscle spindles consist of intrafusal fibers surrounded by a connective tissue capsule. The intrafusal fibers are further divided in nuclear bag fibers (bag1 and bag2) and nuclear chain fibers. Muscle spindles have both sensory and motor innervation. Sensory innervation is provided by group Ia and group II afferents, which terminate in the central region of the muscle spindle. The polar region of the spindles receives motor innervation from gamma motor neurons.

1.3 Pompe disease

Pompe disease (glycogen storage disease type II) is a rare autosomal recessive lysosomal and glycogen storage disorder, which predominantly affects the skeletal muscle, heart, and nervous system (Dasouki et al., 2014; Lim et al., 2014). The disease was first described by Dutch pathologist, Johannes Cassianus Pompe in 1932 (Pompe, 1932). In the same year two German physicians, Bischoff and Putschar, also independently described the disease (Bischoff, 1932; Putschar, 1932). The enzyme which causes the disease was discovered much later in 1963 by Belgian biochemist Henri Hers (Hers, 1963). The incidence of the disease is assumed to be around 1 in 40,000 (Ausems et al., 1999). The cause of Pompe disease are mutations in the *GAA* gene (glucosidase alpha, acid), which encodes the acid α-1,4-glucosidase enzyme (Martiniuk et al., 1991). The GAA enzyme is responsible for breaking down the alpha-1,4- and alpha-1,6-glucosidic linkages of glycogen within lysosomes. So far, more than 600 different mutations have been described (Peruzzo et al., 2019). Mutations that are causative for the disease cause either an absence or a reduced activity of GAA. Since GAA degrades glycogen to glucose, patients with lack of GAA will have glycogen deposited in lysosomes, which cannot be broken down. This then causes the enlargement and destruction of lysosomes and subsequently of the entire cell. Eventually, this leads to malfunctioning of entire organs. It can be assumed that less than about 25% of enzymatic residual activity leads to the symptoms (Niño et al., 2021).

1.3.1 The pathophysiology of muscle damage in Pompe disease

The main mechanism to explain the muscle damage and loss of muscle force in Pompe disease has been the accumulation of glycogen within lysosomes because of the lack of GAA, followed by an enlargement and rupture of the lysosomes, which then causes damage to the contractile apparatus of the muscle. This viewpoint was deemed not complete, especially after it was discovered that enzyme replacement therapy was rather ineffective in treating skeletal muscle damage (Lim et al., 2014). Several pathogenic mechanisms have recently been

suggested to contribute to the pathophysiology of Pompe disease. This includes mechanisms such as: lipofuscinosis, disrupted autophagy, disrupted calcium homeostasis, oxidative stress, and mitochondrial abnormalities (Lim et al., 2014; Kohler et al., 2018; Schoser, 2019). The disruption of the autophagic process, specifically macroautophagy, seems to play a key role specifically in Pompe disease and generally in lysosomal storage diseases (Lieberman et al., 2012; Raben et al., 2012).

1.3.2 Clinical progression and phenotype of Pompe disease

Patients who suffer from Pompe disease have a very variable and heterogeneous course of the disease, which depends on the type of mutation, age of onset and the speed of disease progression. This phenotypic variability has caused difficulties in the classification of the clinical forms, which include classical infantile, late infantile, childhood, juvenile and adult-onset form. However, depending on the age of onset, organ involvement (i.e., cardiomyopathy) and rate of progression, the disease can been broadly classified in infantile-onset Pompe disease (IOPD) and late-onset Pompe disease (LOPD) (Kishnani, Steiner, et al., 2006; Dasouki et al., 2014). Patients with IOPD have an age of onset less or equal to 12 months of age and usually die within the first few years of life. They present with muscle weakness and hypotonia, hypertrophic cardiomyopathy, and respiratory distress (Kishnani, Hwu, et al., 2006).

Patients with LOPD have an age of onset after 12 months of age, have progressive limb-girdle and axial muscle weakness, and usually have no involvement of cardiac muscle (Toscano et al., 2019). In many cases, death is caused by heart failure, respiratory failure, or respiratory infections, such as pneumonia. Rupture of a cerebral aneurysm is also frequently described as the cause of death (Musumeci et al., 2019). The cause are presumably glycogen deposits in arterial vessels.

Although lysosomal glycogen deposition occurs in all tissues, skeletal muscle is particularly affected. This is the main reason why patients suffer from a progressive impairment of motor function, making daily routine activities such as

walking and standing difficult (McIntosh et al., 2015; Valle et al., 2016). The damage to the muscle fibers by the glycogen deposits usually appears shortly after birth. Infants are conspicuous for their flaccid muscle tone, inability to lift their head independently or lack of crawling activity. When the first symptoms appear later, the muscles of the shoulder and pelvic girdle are particularly affected, which affects climbing stairs and lifting the arms above shoulder height. These symptoms worsen as the disease progresses due to the increasing accumulation of glycogen in the muscles. Impairment of the diaphragm leads to breathing problems, which often requires artificial ventilation. Since not only the muscles but also the nerves that supply the muscles are damaged, in late stages there is a reduction or even complete absence of muscle reflexes (areflexia; (Lamartine S Monteiro & Remiche, 2019; Tsai et al., 2019). In addition to the general muscle weakness, patients with Pompe disease show postural symptoms, such as poor stance stability and a swaying gait (Valle et al., 2016). These symptoms lead to balance problems and an increased tendency to fall, resulting in hospitalization and prolonged immobilization, which in turn can exacerbate the symptoms (Grimstone & Hodges, 2003; Horlings et al., 2009). When Pompe disease is suspected, there are different diagnostic tools which can be used including laboratory studies with elevated creatine kinase (CK), elevated liver enzyme levels such as aspartate aminotransferase (AST) and alanine aminotransferase (ALT), elevated urinary glucose tetrasaccharide (Glc4) levels (Young et al., 2012). GAA enzymatic activity can also be measured in IOPD, where the enzyme activity is absent or almost absent (< 1%), whereas low levels of residual activity, up to approximately 25 % of normal, are usually measurable in all other clinical forms. Other diagnostic tests which can be done include muscle biopsy, chest X-rays, electrocardiogram (ECG), echocardiography, spirometry, magnetic resonance imaging (MRI), *GAA* mutation analysis (Kishnani et al., 2013; Dasouki et al., 2014). The primary treatment for GAA deficiency is enzyme replacement therapy (ERT) with Lumizyme ® (alglucosidase alfa). Standard dosing is 20 mg/kg given intravenously every two weeks. (Toscano & Schoser, 2013).

1.4 The mouse model used to study Pompe disease

1.4.1 The *GAA*$^{-/-}$ mouse / B6;129-*Gaa*^{tm1Rabn}/J

For all of my experiments, I used the B6;129-*Gaa*^{tm1Rabn}/J mice (JAX stock #004154; *Gaa*$^{-/-}$ mice) commercially obtained from Jackson Laboratories. These mice are the most widely used preclinical model for Pompe disease and have previously been used in other studies (Bijvoet et al., 1998; Raben et al., 2000; Yi et al., 2017; Colella et al., 2019; Lee et al., 2020). The *Gaa*$^{-/-}$ mouse line was generated by targeting exon 6 of the mouse *GAA* gene with a stop codon and the insertion of a neomycin cassette. Initially, mice that are homozygotes are viable, fertile, have a normal size and weight, and do not display any gross physical or behavioral abnormalities. By three weeks of age, they begin to accumulate glycogen in cardiac and skeletal muscle lysosomes, with a progressive increase thereafter (Raben et al., 1998; Almodóvar-Payá et al., 2020). By 3.5 weeks of age, these mice have markedly reduced mobility and strength. They grow normally, reach adulthood, remain fertile, and, as in the human adult disease, older mice accumulate glycogen in the diaphragm leading to respiratory problems. By 8–9 months of age, animals develop obvious muscle wasting and a weak, waddling gait. As a result, this model reproduces key features of both the infantile and adult forms of the disease. (Bijvoet et al., 1998; Raben et al., 1998).

2. Aim of the study

Some of the symptoms which Pompe patients suffer from include gait and standing instability, which leads to an increased risk of falling (McIntosh et al., 2015; Valle et al., 2016; Lamartine S Monteiro & Remiche, 2019). The study by Schneider et al. reported that this instability could be only partially explained by the reduced muscles strength as a results of the underlying myopathy (Schneider et al., 2020). It is therefore possible that patients with Pompe disease have an altered proprioception.

To test this hypothesis, I investigated the morphology of muscle spindles of *Gaa*$^{-/-}$ mice quantitatively and qualitatively, since muscle spindles are the main proprioceptors. More specifically, I investigated muscle spindle morphology in 2.5-month-old and 8.5-month-old wildtype and *Gaa*$^{-/-}$ mice and compared them to C57BL/6 wildtype mice. To determine if the muscle fiber type composition plays a role in the degeneration of the muscle spindle structure, I examined the slow twitch soleus muscles and the fast twitch EDL muscle.

The following parameters were quantified:

1) the width and length of circumferential elements of the sensory afferents of the muscle spindles in the Soleus and EDL muscle in 2.5-month-old and 8.5-month-old wildtype and *Gaa*$^{-/-}$ mice.

2) the number of intrafusal sarcomeres per µm in the soleus and EDL muscle in 2.5-month-old and 8.5-month-old wildtype and *Gaa*$^{-/-}$ mice

3) the number of muscles spindles in the soleus muscle in wildtype and *Gaa*$^{-/-}$ mice.

3. Materials and Methods

3.1 Materials

3.1.1 Chemicals

Table 1. List of Chemicals used

Chemical	Company	Catalog number
4',6-Diamidino-2-phenylindole dihydrochloride (DAPI)	Carl Roth GmbH & Co. KG, Karls-ruhe,Germany	6335.1
Albumin Fraction V	Carl Roth GmbH & Co. KG, Karlsruhe, Germany	8076.2
Aqua-Poly/Mount	Polysciences, Inc. Europe GmbH	18606
D-Glucose	Sigma-Aldrich Chemie GmbH, Taufkirchen, Germany	G5146
Goat Serum	Thermo Fisher Scientific Inc.	50197Z
KCl	Carl Roth GmbH & Co. KG, Karlsruhe, Germany	6781.3
KH_2PO_4	Carl Roth GmbH & Co. KG, Karls-ruhe,Germany	3904.1
NaCl	Carl Roth GmbH & Co. KG, Karlsruhe, Germany	9265.1
$NaHCO_3$	Carl Roth GmbH & Co. KG, Karlsruhe, Germany	6885.1
Paraformaldehyde	Carl Roth GmbH & Co. KG, Karlsruhe, Germany	0335.1
Tissue Tec®	Sakura Finetek Europe, AJ Alphen an denRijn, Netherland	TTEK
Tween20	Carl Roth GmbH & Co. KG, Karlsruhe, Germany	9127.1
Xylazine	Bayer AG, Leverkusen, Germany	

3.1.2 Antibodies

3.1.2.1 Primary Antibodies

Table 2. List of primary antibodies

Antibody	Host	Dilution	Company	Catalog number
Anti-light chain 3-like protein (LC3A/B)	Rabbit	1:500	Thermo Fisher	PA1-16931
Anti-myosin heavy chain 6 (S46)	Mouse	1:200	Developmental Studies Hybrid-oma Bank	
Anti-$Na_V1.4$	Rabbit	1:500	Alomone Labs	ASC-020
Anti-vesicular glu-tamate transporter 1 (vGluT1)	Guinea pig	1:500	Millipore	AB5905

3.1.2.2 Secondary Antibodies

Table 3. List of secondary antibodies

Antibody	Host	Dilution	Company	Catalog number
Anti-Guinea pig Alexa Flour 488	Goat	1:1000	Thermo Fisher	A-11073
Anti-Mouse Alexa Flour 647	Goat	1:1000	Thermo Fisher	A-21235
Anti-Rabbit Alexa Flour 594	Goat	1:1000	Thermo Fisher	A-11012

3.1.3 Computer programs

Table 4. List of computed programs

Software	Company
Adobe Photoshop	Adobe Inc.
ImageJ	public domain Java image processing program from NIH, USA
Inkscape	Inkscape Project - free and open-source vector graphics editor (https://inkscape.org/)
Microsoft Excel	Microsoft Corporation
Zeiss Software	Zeiss

3.1.4 Mice

Table 5. List of mice used

Line	Producer/Manufacturer	Quantity
B6;129-*Gaa*^{tm1Rabn}/J	The Jackson Laboratory (JAX stock #004154)	Three 2.5-month-old *Gaa*$^{-/-}$ mice Three 8.5-month-old *Gaa*$^{-/-}$ mice All mice were female
C57BL6/J	The Jackson Laboratory (JAX stock #000664)	Three 2.5-month-old BL6 mice Three 8.5-month-old BL6 mice All mice were female

3.1.4.1 The C57BL/6J mouse / Control group

B6;129-*Gaa*^{tm1Rabn}/J mice were used as experimental animals. As the control group, I used the C57BL/6J mice (JAX stock #000664). Both strains were bred at the animal facility of the Biomedical Center. Three 2.5-month-old BL6 mice and three 8.5-month-old BL6 mice were used. All mice were female. The recommended control group for *Gaa*$^{-/-}$ mice is the B6129SF1/J mice. Unfortunately, these mice were not available during my study, and we therefore used C57BL/6J mice as controls. This appears acceptable since previous studies have shown

that there is little if any morphological difference in the structure of muscle spindles in different mouse lines (Lionikas et al., 2013), allowing the comparison between these two mouse strains. However, there are differences between the mice lines regarding their behavior and weight.

3.1.5 Buffers and solutions

Table 6. 10x Phosphate-Buffered Saline (PBS) Recipe

Na_2HPO_4	17.8 g
KH_2PO_4	2.4 g
NaCl	80 g
KCl	2 g
Milli-Q® Water	1 L

Table 7. 1x Phosphate-Buffered Saline (PBS) Recipe

10x Phosphate-Buffered Saline	100 ml
Milli-Q® Water	900 ml

Table 8. Phosphate-Buffered Saline with Tween (PBS-T) Recipe

10x Phosphate-Buffered Saline	100 ml
Milli-Q® Water	900 ml
Tween® 20	100 µl

Table 9. Blocking Solution Recipe for 50ml

Phosphate-Buffered Saline with Tween	44.75 ml
ROTI®ImmunoBlock	5ml µl
Goat serum	250 µl
Bovine serum albumin	0.5 g

All chemicals (unless stated otherwise) were commercially purchased from Sigma/Aldrich

3.2 Methods

3.2.1 Fixation and perfusion of animals

In order to obtain muscle tissue for immunohistochemistry, fixation of the mice was performed using transcardial perfusion by Jürgen Schultheiß. Mice were deeply anaesthetized using ketamine and xylazine. Using a forceps, pedal reflexes were evaluated to determine the level of anesthesia. When no reflex response and no pain response could be detected, the mice were perfused with fixative while stretched on a styrofoam plate. After opening the thorax and exposing the heart, a needle was placed in the left ventricle. Then the right atrium was opened, and PBS was pumped through the vascular system at a rate of 3 ml/min for 2 minutes. When the color of the liver became brighter, that served as an indication of successful cleaning of the vasculature. The perfusion solution was then switched to 4% paraformaldehyde fixative solution (PFA), which was perfused into the mice for 20 minutes at the same rate.

To obtain muscle tissue, the posterior extremities were skinned. The soleus and EDL muscles were carefully dissected from the fixed hind legs and then incubated in a 30% sucrose in PBS solution overnight to osmotically remove water. Afterwards, the muscles were embedded in Tissue Tec® and frozen at -20 °C. The tissue was then cryo-sectioned using the cryostat (Epredia™ CryoStar cryostat NX70, Thermo Fisher Scientific Inc., Massachusetts, USA) at temperatures between -18°C and -20°C at 25 µm thickness. Muscle sections were collected on Epredia™ SuperFrost Plus™ slides (Thermo Fisher Scientific Inc., Massachusetts, USA) and stored at -20°C.

3.2.2 Immunohistochemistry

Frozen sections were thawed at room temperature for 30 minutes, encircled with special marking pen that provides a hydrophobic barrier (Pap-Pen, Vector Laboratories, Burlingame, USA) and washed 10 min in phosphate buffered saline (PBS) (for recipe see Table.7) to remove the Tissue Tec®. Afterwards the sections were washed 3 times for 10 min each in phosphate buffered saline with

Tween (PBS-T) to reduce the cell membrane integrity and expose the antigenic sites. In order to reduce unspecific binding of antibodies and to eliminate residual PFA, the sections were incubated in blocking solution for 1 hour at room temperature. Afterwards, the sections were incubated overnight with the primary antibodies diluted in blocking solution. On the next day, sections were washed 3 times in PBS-T for 10 minutes each and afterwards incubated for 1 hour with the corresponding secondary antibody, diluted in blocking solution. Sections were then washed 10 min in PBS and the nuclei were stained using 4', 6' diamidino-2-phenylindoles (DAPI) at a concentration of 2 µg/ml in blocking solution for 10 min. This was followed by two washing steps in PBS for 10 minutes each. The slides were then embedded in Aqua-Poly/Mount mounting medium and covered with a cover slip. To demonstrate the specificity of the staining, negative controls were run in parallel. In the negative control, the primary antibody was omitted, and the incubation of the sections was done only with the secondary antibody. It should be noted that there was some variation in how the muscle spindles appeared after taking confocal images due to the different steps of IHC and the staining variability (i.e., perfusion, fixation, cryosectioning, incubation). A standardized protocol for perfusion and immunohistochemistry was used to reduce the variability.

3.2.2.1 Epifluorescence microscopy

To determine the number and location of muscle spindles in the muscle sections, the Zeiss Microscope Axio Imager M2 epifluorescence microscope was used. The soleus muscle from three animals for each genotype were completely sectioned and stained with antibodies against vGluT1 as described above. The number of muscle spindles for each individual soleus muscle was manually counted as described by Gerwin et al., 2020. Muscle spindles were identified by morphological criteria, such as a positive staining of the annulospiral endings with vGluT1 and positive staining with DAPI showing the characteristic distribution of the nuclei within the intrafusal bag and chain fibers. The subsequent more detailed investigation of the muscle spindle was performed using the confocal microscope.

3.2.2.2 Confocal microscopy

Muscle spindles were further analyzed using a Zeiss LSM 710 laser scanning confocal microscope. The Zeiss LSM 710 was equipped with four lasers: Diode 405-30 (405 nm, 30.0 mW), HeNe laser (633 nm, 5.0 mW), DPSS laser (561 nm, 15.0 mW) and Argon laser (488 nm, 25.0 mW). For muscle spindle images, a 40x water immersion objective (LD C-Apochromat 40x/1.1) was used. In addition, the Z-stack function was used with a stack thickness of 10-15µm and interval thickness of 1µm. A scanning speed of 5 (pixel time) with a 1024x1024 resolution was used. The images were saved in the CZI file format.

3.2.3 Data analysis

The Java image processing program software package Fiji – ImageJ was used to digitally process and analyze entire images, including adjusting brightness and contrast. (Eliceiri et al., 2012; Schindelin et al., 2012). Each of the confocal z-stack images was reduced to one plane using the maximum intensity projection function. This allowed the detailed examination of the circumferential elements of the sensory nerve terminals in the equatorial region and the sarcomeres in the polar regions of the muscle spindle. For each confocal image of a muscle spindle, the intrafusal fibers were identified as a bag or chain fiber and their number was counted. After the identification, the length and width of the circumferential elements of each intrafusal bag and chain fiber was determined. The number of sarcomeres per µm for every intrafusal fiber was also determined. To this end, a line was drawn in the contractile part of the intrafusal fiber and all the sarcomeres within the line were counted. The number of sarcomeres was then divided by the length of the line. Figure 2 shows an example on how the measurements were done. All statistical analyses were performed by using Microsoft Excel. The level of significance (P-value) for all statistical tests was set at *$P < 0.05$, **$P < 0.01$, ***$P < 0.001$ using the Student's t-test.

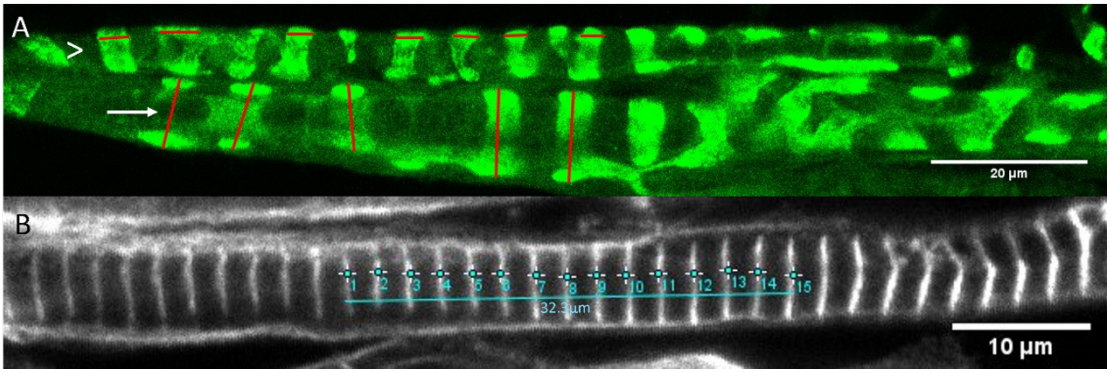

Figure 2. Figure of a muscle spindle showing how the measurements were done using the Fiji – ImageJ program. Panel A shows circumferential elements which were marked with anti-vGluT1 antibody. The white arrowhead indicates how the width measurements were done. The white arrow shows how the length measurements were done. Panel B shows the sarcomeres which were stained using the S46 antibody against myosin heavy chain 6. To measure the sarcomeres per µm a line was drawn within the contractile part of the muscle spindle and the number of sarcomeres within that line was counted. Scale bars: A, 20 µm; B, 10µm

4. Results

4.1 Qualitative Analysis of Muscle Spindle Morphology

To investigate if the lack of the GAA enzyme affects the structure of muscle spindles, I used different antibodies to identify changes in the distribution of specific marker proteins in wildtype and *Gaa*$^{-/-}$ muscle spindle. The anti-vesicular glutamate transporter (vGluT1) antibody was used to identify the sensory neuron with its annulospiral endings (Zhang, 2014), the S46 antibody which marks the myosin heavy chain 6 specifically in nuclear bag fibers (Miller et al., 1985), the anti-$Na_v1.4$ antibody which marks the voltage-gated sodium channel $Na_v1.4$ (Watkins et al., 2022). Since the symptoms for the disease usually worsen with age of the mice (Raben et al., 1998), the muscle spindles of 2.5-month-old and 8.5-month-old mice were compared to determine the disease progression. Mice that were older that 8.5-month-old were not used, to avoid unnecessary animal suffering, as older mice usually develop convulsions (Raben et al., 2000).

4.1.1 Muscle Spindle Morphology of 2.5-Month-Old Mice

Since Pompe disease is characterized by a steady progressive muscle damage and degeneration, the muscle spindle morphology of 2.5-month-old *Gaa*$^{-/-}$ mice was investigated first, followed by the investigation in 8.5-month-old *Gaa*$^{-/-}$ mice to see how the disease progression affects muscle spindles. Figure 3 shows the morphology of a representative muscle spindle from 2.5-month-old wildtype mice in the extensor digitorum longus muscle (EDL). The vGlut1 staining indicates the presence of the circumferential elements in the nuclear bag and chain fibers. The S46 and $Na_v1.4$ staining shows the distribution of the sarcomeres in the polar regions of the muscle spindle. The distribution of all three antigens was identical to what has been described previously (Pedrosa et al., 1990; Kucera et al., 1992; Walro & Kucera, 1999; De-Doncker et al., 2002; Zhang, 2014; Gerwin et al., 2019; Watkins et al., 2022). The S46 staining was only observed in the polar regions of the nuclear bag fibers, since it is specific for nuclear bag fiber

(Kucera & Walro, 1995). In contrast, the $Na_v1.4$ staining was present in both nuclear bag and chain fibers but due to the sarcomeres being concentrated in the polar region, the equatorial region was mostly devoid of staining. The 4′,6-diamidino-2-phenylindole (DAPI) staining shows a distribution of the nuclei similar to what has been described before (Gerwin et al., 2020; Kröger & Watkins, 2021). The muscle spindle in Fig. 3 consisted of a nuclear bag fiber characterized by the aggregated nuclei and a nuclear chain fiber characterized by the chain-like alignment of the nuclei. In summary, this shows an intact muscle spindle morphology in 2.5-month-old control mice.

I next compared the distribution of the different marker proteins in muscle spindles from control animals to spindles from *Gaa*$^{-/-}$ mice. Figure 4 shows the muscle spindle morphology of 2.5-month-old *Gaa*$^{-/-}$ mice in the EDL muscle. The muscle spindle in this case was also intact, including the presence of the circumferential elements in the sensory nerve terminals, the presence of sarcomeres in the polar regions and a normal distribution of the nuclei. In conclusion, I did not detect major obvious differences between the muscle spindle morphology of the 2.5-month-old wildtype and 2.5-month-old *Gaa*$^{-/-}$ mice. There were also no apparent differences observed in the muscle spindle morphology between 2.5-month-old *Gaa*$^{-/-}$ and age-matched control mice in the slow-twitch soleus muscle (data not shown).

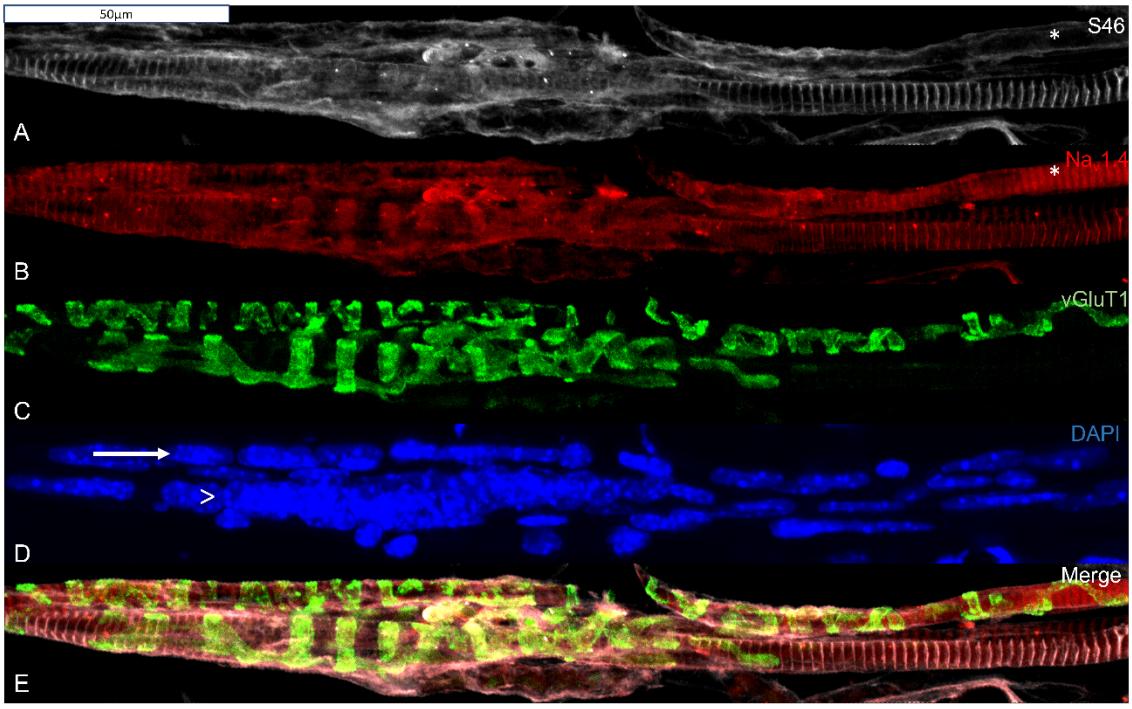

Figure 3. Muscle Spindle of 2.5-month-old Wildtype Mice in the EDL Muscle.

(A) Staining against myosin heavy chain 6 with S46 antibody shown in the polar regions of the nuclear bag fiber. The absence of S46 antibody in the central region of the spindle is due to the very few sarcomeres, which are present as circumferential ring in the subsarcolemmal region. Note here also the lack of staining of the intrafusal chain fiber marked with asterisk. (B) Likewise, antibodies against sodium channel $Na_v1.4$ stain the polar regions of nuclear bag fiber and chain fibers of the muscle spindle. Anti-$Na_v1.4$ antibody is similarly absent in the central region of the spindle is due to the very few sarcomeres in this region. (C) Staining using antibodies against vesicular glutamate transporter 1 (vGluT1) showing the circumferential elements of sensory nerve terminals. (D) Cell nuclei labelled with DAPI. In the nuclear chain fiber (marked by the arrow in panel D), the nuclei are aligned one after another, whereas in the nuclear bag fiber (marked by an arrowhead in panel D) the nuclei are aggregated on top of each other. (E) Merge of the panels Scale bar: 50µm.

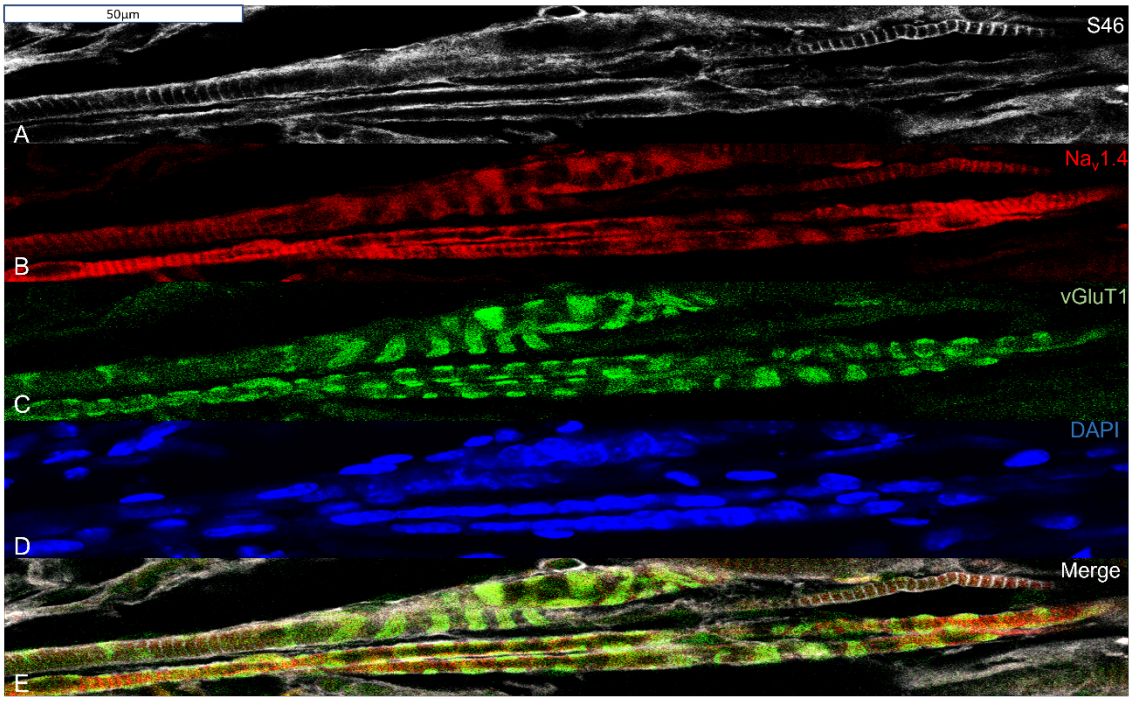

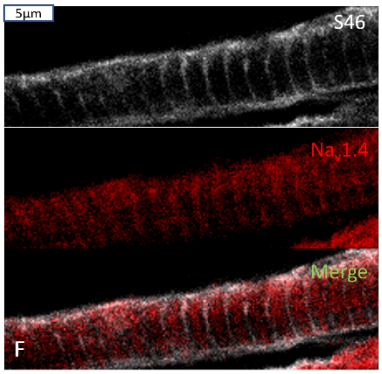

Figure 4. Muscle Spindle of 2.5-month-old *Gaa*$^{-/-}$ Mice in the EDL Muscle. Distribution of different molecular markers showing an intact muscle spindle. (A) Staining against myosin heavy chain 6 with S46 antibody shown in the polar regions of the nuclear bag fiber. (B) Staining against Na$_v$1.4 using anti-Na$_v$1.4 antibody stain the polar regions of nuclear bag fiber and chain fibers of the muscle spindle. (C) Staining of the circumferential elements of sensory terminals with anti-vGluTt1 antibody. (D) Nuclei stained with DAPI show two nuclear bag and two chain fibers. (E) Merge of the panels (minus panel D) showing a non-overlapping distribution of Anti-Na$_v$1.4 and S46 antibody in the polar regions of nuclear bag fiber. Scale bar: 50µm. (F) Higher magnification of the distribution of S46 and Na$_v$1.4 in a peripheral part of an intrafusal fiber. Scale bar: 5µm.

4.1.2 Muscle Spindle Morphology in 8.5-Month-Old Mice

The next age groups of mice I investigated were the 8.5-month-old wildtype and *Gaa*$^{-/-}$ mice. Figure 5 shows the muscle spindle morphology in the EDL muscle of a 8.5-month-old wildtype mouse. The muscle spindle morphology of the 8.5-month-old wildtype mice was similar to the 2.5-month-old wildtype mice and to what has been described before (Gerwin et al., 2020; Watkins et al., 2022). This includes the presence of circumferential elements marked by vGluT1 in the central region of the spindle, the presence of the sarcomeres in the polar regions of the muscle spindle shown by the S46 and $Na_v1.4$ staining and lastly a normal distribution of intrafusal fiber cell nuclei.

I next compared the morphology of muscle spindles from 8.5-month-old wildtype mice with that of 8.5-month-old *Gaa*$^{-/-}$ mice. Figure 6 shows a muscle spindle from a 8.5-month-old *Gaa*$^{-/-}$ mouse. Here the morphology of the muscle spindle was clearly disrupted. In the center of the muscle spindle, there was a total lack of the circumferential elements of the sensory nerve terminals of the muscle spindle. Instead, vGluT1 immunoreactivity labeled multiple large varicosities (shown by white arrows in Fig.6C). In addition, the nuclei of the intrafusal fibers were not as clearly arranged in the standard chain or bag fiber pattern, suggesting an abnormal distribution of nuclei (shown in Fig.6D). The sarcomeres were still present in the polar region of the muscle spindle (Fig.6A and Fig.6B). The same differences were also observed in the muscle spindle morphology of the slow-twitch soleus muscle (data not shown).

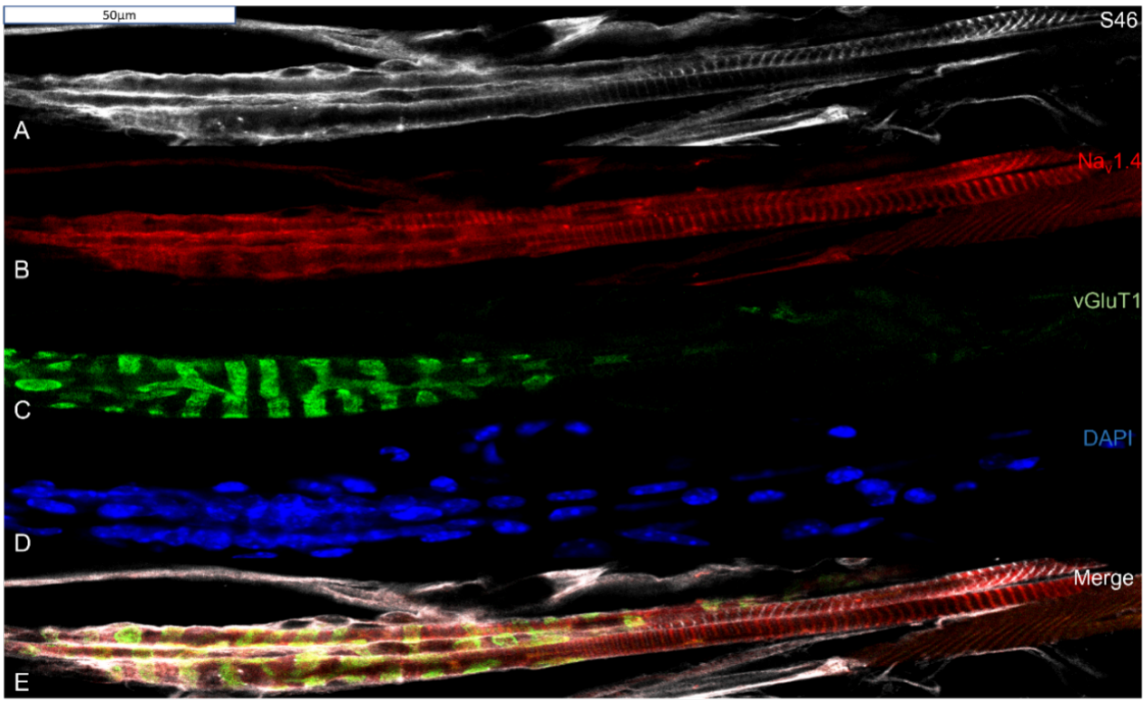

Figure 5. Muscle Spindle of 8.5-month-old Wildtype Mice in the EDL Muscle.

Distribution of different molecular markers showing an intact muscle spindle. (A) Staining against myosin heavy chain 6 with S46 antibody shown in the polar regions of the nuclear bag fiber. (B) Likewise, staining against Nav1.4 using anti-Nav1.4 antibody stain the polar regions of nuclear bag fiber and chain fibers of the muscle spindle. (C) Staining of the circumferential elements of sensory terminals with anti-vGluTt1 antibody. (D) Nuclei stained with DAPI. (E) Merge of all panels (minus panel D). Scale bar: 50µm.

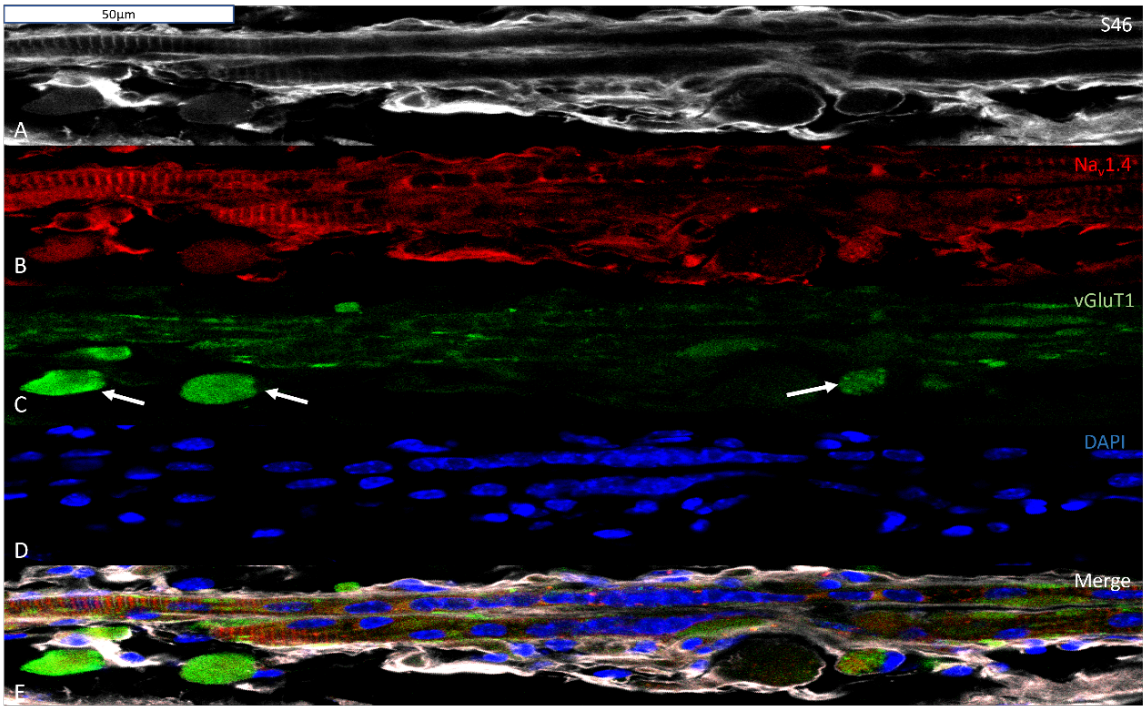

Figure 6. Muscle Spindle of 8.5-month-old *Gaa*$^{-/-}$ Mice in the EDL Muscle.

Distribution of different molecular markers, indicating muscle spindle degeneration. (A) Staining against myosin heavy chain 6 with S46 antibody showing the sarcomeres still present in the polar region the muscle spindle. (B) Likewise, staining against $Na_v1.4$ using anti-$Na_v1.4$ antibody showing the sarcomeres still present in the polar region the muscle spindle. (C) Staining of the sensory terminals with anti-vGluT1 showing a complete lack of the circumferential elements and the presence of varicosities (indicated by the white arrow). (D) Nuclei stained with DAPI. The nuclei are not as clearly arranged in the typical bag and chain fiber pattern. (E) Merge of all panels. Scale bar: 50µm.

4.2 Autophagic Build-up in Muscle Spindles of *Gaa*$^{-/-}$ Mice

Autophagy is an intracellular degradation system that delivers cytoplasmic constituents to the lysosome, where they are degraded and recycled (Mizushima, 2007). Since it is known that the autophagic process is disrupted and there is an accumulation of autophagosomes in extrafusal fibers of *Gaa*$^{-/-}$ mice and patients with Pompe disease (Lim et al., 2014; Kohler et al., 2018), I investigated if there is autophagic buildup also in intrafusal fibers of the muscle spindles from *Gaa*$^{-/-}$ mice. To this end the specific autophagosome marker microtubule-associated proteins 1A/1B light chain 3 (also known as LC3) (Kabeya et al., 2000) was used. The muscle spindles of 2.5-month-old wildtype mice and *Gaa*$^{-/-}$ mice as well as 8.5-month-old wildtype mice and *Gaa*$^{-/-}$ mice were analyzed. Figure 7B shows a muscle spindle of a 2.5-month-old wildtype mouse in the EDL muscle, where there was no evidence of autophagic build-up. In contrast, in the 2.5-month-old *Gaa*$^{-/-}$ mice a few autophagic vacuoles were detectable (Fig. 8). Figure 9 shows a representative muscle spindle of 8.5-month-old wildtype mice, where no autophagic build-up was observed. In contrast, the muscle spindle of 8.5-month-old *Gaa*$^{-/-}$ mice (Fig.10) showed considerable autophagic build-up. Similar results were obtained when I analyzed the muscle spindles in the 2.5-month-old and 8.5-month-old *Gaa*$^{-/-}$ mice of the slow-twitch soleus muscle (data not shown). These results show that the intrafusal fibers in *Gaa*$^{-/-}$ mice are similarly affected by the autophagic build-up as are the extrafusal fibers. Furthermore, it appears that a disruption of autophagy might begin in mice as early as 2.5-months of age.

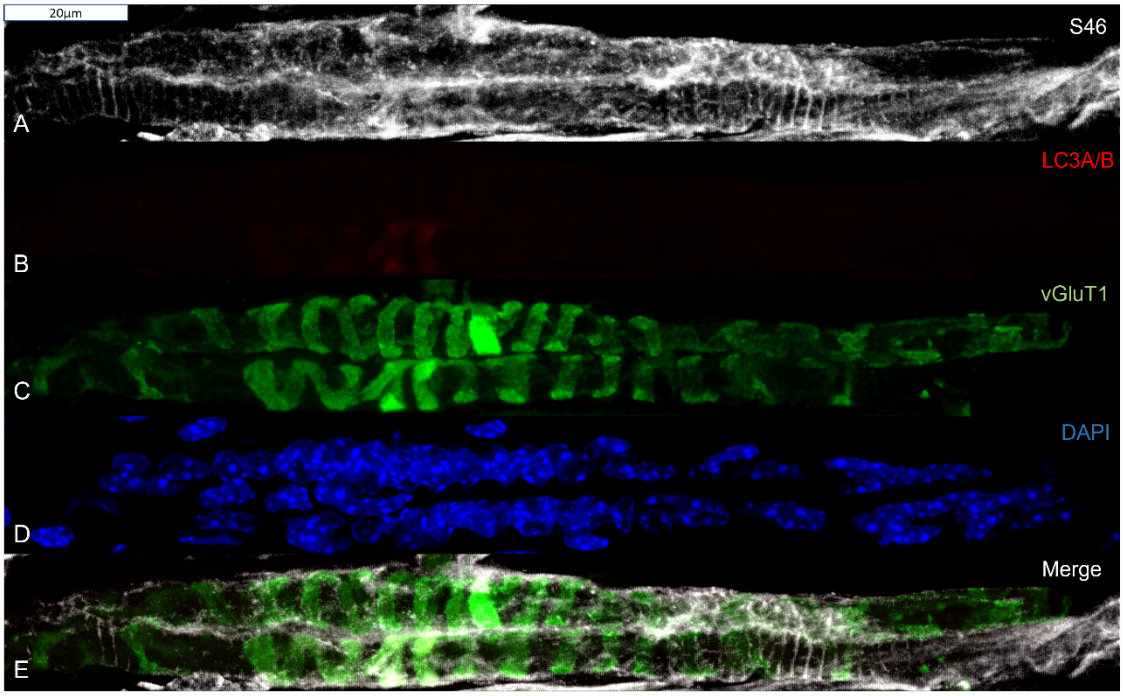

Figure 7. Distribution of LC3A/B in Muscle Spindle of 2.5-month-old Wildtype Mice in the EDL Muscle. Distribution of molecular markers showing an intact muscle spindle and no autophagic accumulation. (A) Staining against myosin heavy chain 6 with S46 antibody shown in the polar regions of the nuclear bag fiber. (B) Staining of the autophagosomes with LC3A/B antibody showing no autophagic accumulation. (C) Staining of the circumferential elements of the sensory terminal with vGluT1. (D) Nuclei stained with DAPI. (E) Merge of all panels (minus panel D). Scale bar: 20µm.

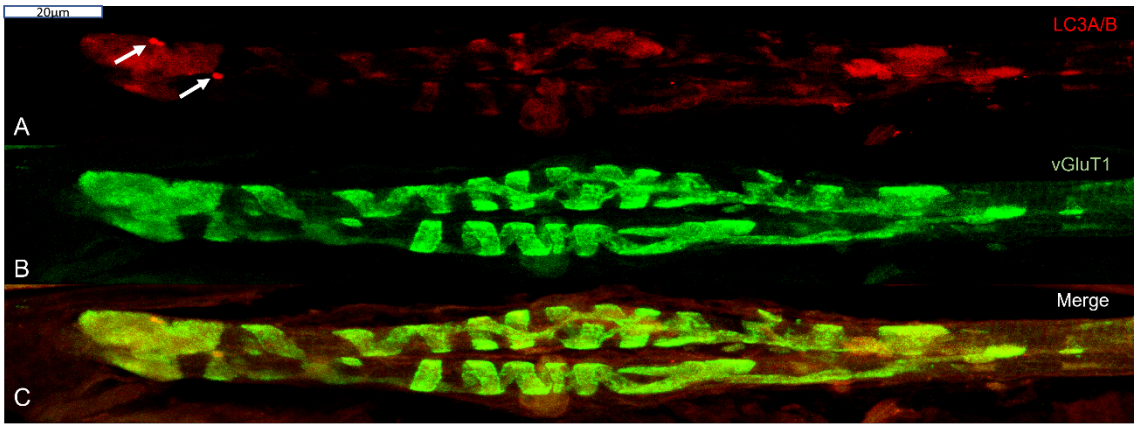

Figure 8. Distribution of LC3A/B in Muscle Spindle of 2.5-Month-Old *Gaa*$^{-/-}$ Mice in the EDL Muscle Distribution of molecular markers showing an intact muscle spindle with little to no autophagic

accumulation. (A) Staining of the autophagosomes with LC3A/B antibody showing some autophagic vacuoles marked by white arrows (B). Staining of the sensory terminals with vGluT1, showing the circumferential elements still intact. (C) Merge of the panels showing colocalization of LC3A/B antibody with the sensory nerve terminal, suggesting that the terminal is degrading first before the intrafusal fiber. Scale bar: 20μm.

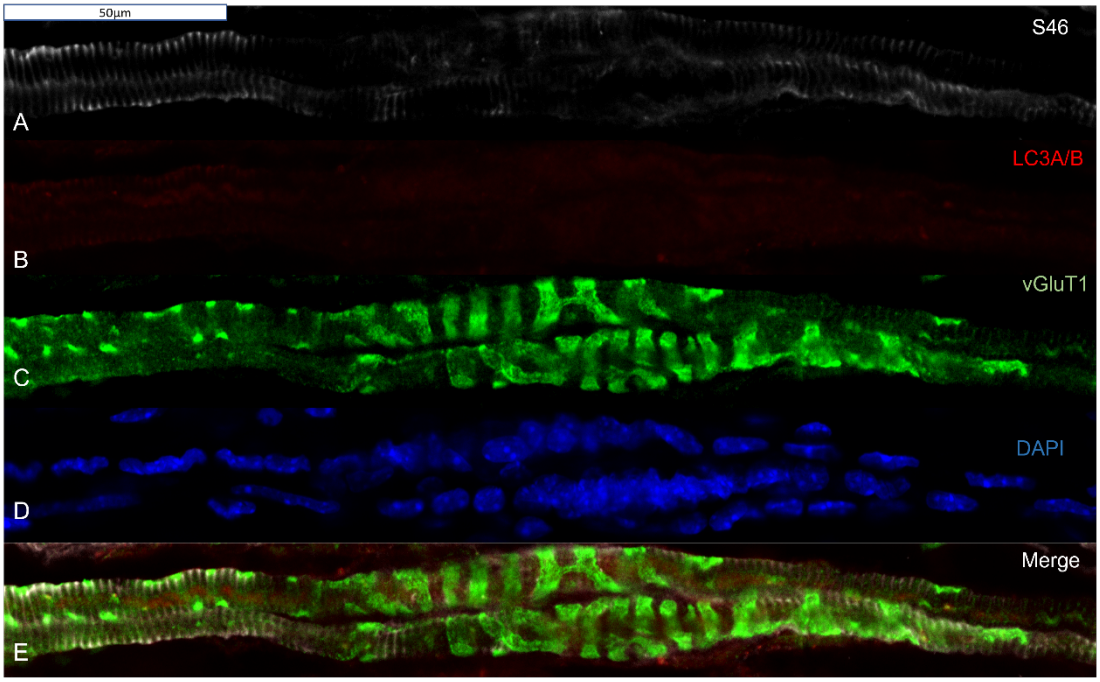

Figure 9. Distribution of LC3A/B in Muscle Spindle of 8.5-Month-Old Wildtype Mice in the EDL Muscle. Distribution of molecular markers showing an intact muscle spindle and no autophagic accumulation. (A) Staining against myosin heavy chain 6 with S46 antibody shown in the polar regions of the muscle spindle. (B) Staining of autophagosomes with LC3A/B antibody showing no autophagic build-up. (C) Staining of the sensory terminals with vGluTt1, showing the circumferential elements still intact (D) Nuclei stained with DAPI. (E) Merge of all panels (minus panel D). Scale bar: 50μm.

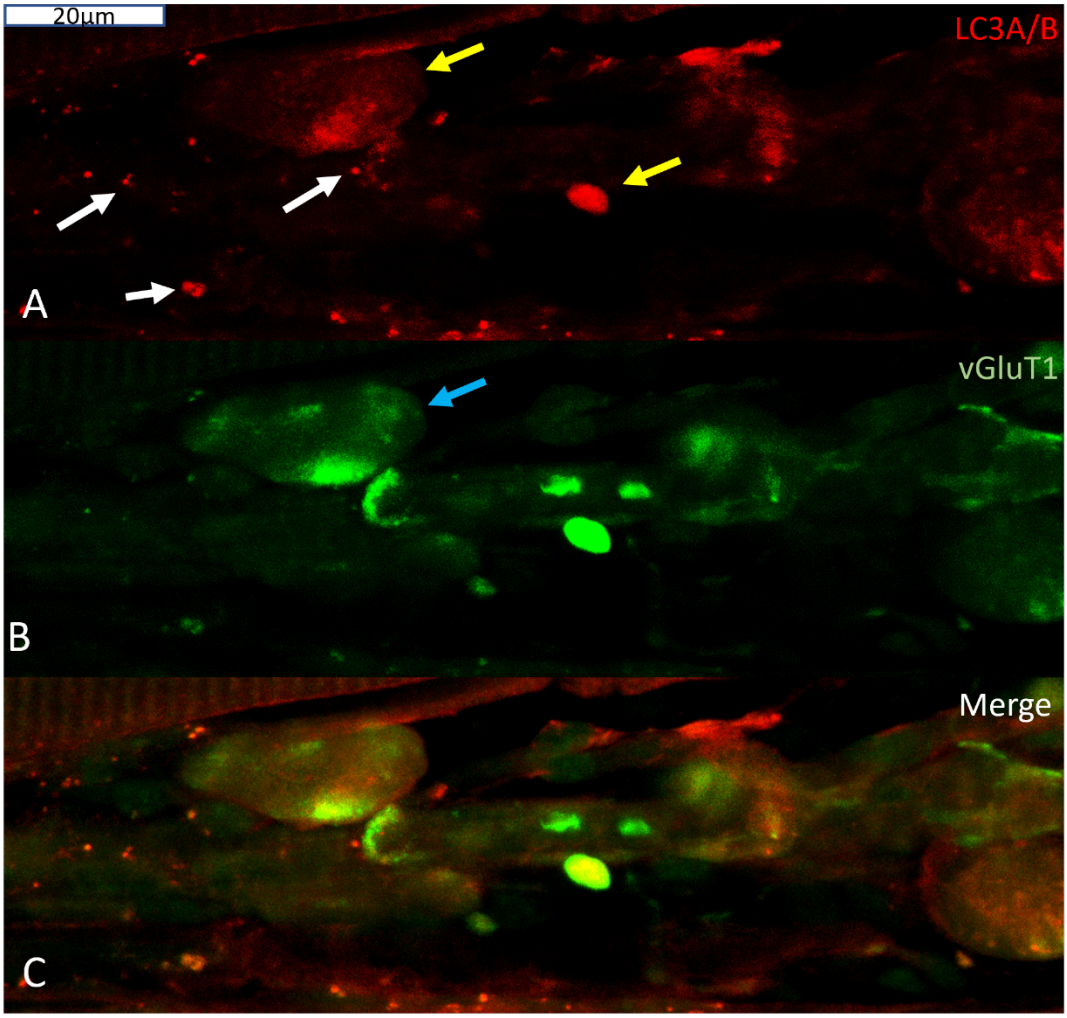

Figure 10. Distribution of LC3A/B in Muscle Spindle of 8.5-month-old *Gaa*$^{-/-}$ in the EDL Muscle. Distribution of molecular markers, showing muscle spindle degeneration and autophagic accumulation inside the muscle spindle. (A) Staining of the autophagosomes with LC3A/B antibody showing considerable autophagic build-up inside the intrafusal fiber marked by the white arrows and inside the vGluT1-positive varicosity marked by the yellow arrows. (B) Staining of the sensory terminals with anti-vGluT1 antibodies showed a complete lack of the circumferential elements and the presence of a varicosity marked by the blue arrow. (C) Merge of all panels. Scale bar: 20µm.

4.3 Quantitative Analysis

4.3.1 Width and Length of Circumferential Elements in Bag and Chain Fibers

Muscle spindles from different mice and different muscles showed a different degree of degeneration, so it was necessary to quantify the immunohistochemistry results. Therefore, I conducted a quantitative analysis to investigate if there was any difference in the morphology of the circumferential elements of the sensory nerve terminals in the wildtype mice and *Gaa*$^{-/-}$ mice. Both the width and length of the circumferential elements of the sensory terminals in the nuclear bag fiber and the nuclear chain fiber in the 2.5-month-old wildtype mice and *Gaa*$^{-/-}$ mice were analyzed in the slow twitch soleus muscle and fast twitch EDL muscle. Figure 11 shows the differences in the width and length of the circumferential elements in nuclear bag and chain fibers in the EDL muscle between the 2.5-month-old wildtype and *Gaa*$^{-/-}$ mice. I observed that in the nuclear bag fibers, the circumferential elements had a greater width in *Gaa*$^{-/-}$ mice compared to the wildtype mice. In contrast, the length of the circumferential elements in the nuclear bag fibers, was shorter in the *Gaa*$^{-/-}$ mice compared to control mice. Similar results in the circumferential elements of nuclear chain fibers were also observed in the EDL muscle between the 2.5-month-old wildtype and age-matched *Gaa*$^{-/-}$ mice. The mean values for the length and width of the circumferential elements in the EDL muscle for the *Gaa*$^{-/-}$ and BL6 lines are given in Table 10 together with the corresponding standard deviations. Figure 12 shows the differences in the width and length of the sensory nerve terminal circumferential elements in nuclear bag and chain fibers from the soleus muscle of 2.5-month-old wild type and *Gaa*$^{-/-}$ mice. Here I also observed that in both the nuclear bag fibers and nuclear chain fibers, the circumferential elements had a greater width in the *Gaa*$^{-/-}$ mice compared to the control mice. In contrast, the length of the circumferential elements in the nuclear bag and chain fibers, was shorter in the *Gaa*$^{-/-}$ mice compared to wildtype mice. The mean values for the length and width of the circumferential elements in the soleus muscle for the *Gaa*$^{-/-}$ and BL6 lines are given in Table 11

together with the corresponding standard deviations. These results show that the circumferential elements of the sensory terminals in the EDL and soleus muscle in 2.5-month-old mice get wider and shorter. Comparing the circumferential elements of the muscle spindles between the wildtype group and *Gaa*$^{-/-}$ mice was not possible, because of the complete lack of the circumferential elements in the muscle spindles of 8.5-month-old *Gaa*$^{-/-}$ mice due to the degeneration of the sensory nerve terminal.

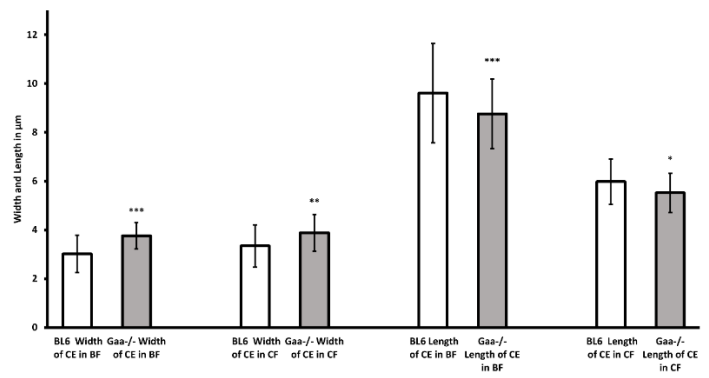

Figure 11. Width and Length of Circumferential Elements in Bag and Chain Fibers in 2.5-month-old BL6 and *Gaa*$^{-/-}$ Mice in the EDL Muscle. In the EDL muscle of *Gaa*$^{-/-}$ mice the circumferential elements of sensory nerve terminals were significantly wider and shorter in the nuclear bag and chain fibers when compared to the CE of the sensory nerve terminals of BL6 mice. Mean ± Standard deviation; BL6: N=3 mice, n=9 spindles; *Gaa*$^{-/-}$: N=3 mice, n=9 spindles; Student 's t-test, P-values: *<0.05, **<0.01, ***<0.001; CE: Circumferential Elements, BF: Bag Fibers, CF: Chain Fibers.

Table 10. Mean Values (Width and Length in µm) and ± STDEV of the Circumferential Elements in Bag and Chain Fibers in BL6 and *Gaa*$^{-/-}$ Mice of EDL Muscle.

EDL Muscle					
	BL6		*Gaa*$^{-/-}$		
	Mean	± STDEV	Mean	± STDEV	P-Value
Width of CE in Bag fibers	3.01	0.76	3.76	0.54	0.0001
Width of CE in Chain fibers	3.34	0.87	3.89	0.75	0.0019
Length of CE in Bag fiber	9.61	2.04	8.77	1.43	0.0008
Length of CE in Chain fibers	5.98	0.94	5.52	0.81	0.015

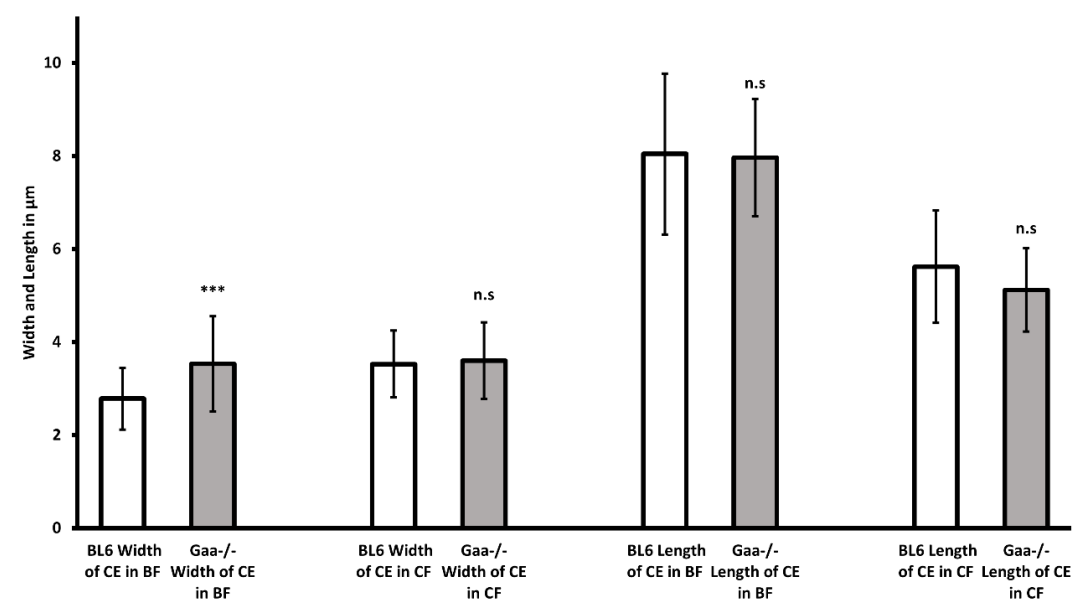

Figure 12. Width and Length of Circumferential Elements in Bag and Chain Fibers in 2.5-month-old BL6 and *Gaa*$^{-/-}$ Mice in the Soleus Muscle. In the soleus muscle of *Gaa*$^{-/-}$ mice only the width of CE of the sensory nerve terminals in the nuclear bag fibers was significantly greater when compared to CE of sensory nerve terminals of BL6 mice. Mean ± Standard deviation; BL6: N=3 mice, n=9 spindles; *Gaa*$^{-/-}$: N=3 mice, n=9 spindles; Student's t- test, P-values: *<0.05, **<0.01, ***<0.001; CE: Circumferential Elements, BF: Bag Fibers, CF: Chain Fibers.

Table 11. Mean Values (Width and Length in µm) and ± STDEV of the Circumferential Elements in Bag and Chain Fibers in BL6 and *Gaa*$^{-/-}$ Mice of Soleus Muscle.

Soleus Muscle					
	BL6		*Gaa*$^{-/-}$		
	Mean	± STDEV	Mean	± STDEV	P-Value
Width of CE in Bag fibers	2.78	0.67	3.53	1.02	0.0001
Width of CE in Chain fibers	3.53	0.72	3.60	0.82	0.7108
Length of CE in Bag fiber	8.05	1.73	7.96	1.25	0.716
Length of CE in Chain fibers	5.62	1.21	5.12	0.89	0.085

4.3.2 Quantitative Analysis of the Number of Muscle Spindles per Muscle

To investigate if muscle spindles are also affected by degeneration in the GAA deficient mice, resulting in muscle spindle loss, I determined the number of muscle spindles in the soleus muscles and compared these values between wildtype and *Gaa*$^{-/-}$ mice. The results are shown in Figure 13. The mean number of muscle spindles in the 8.5-month-old wild type mice was 8.25, compared to 4.67 in the 8.5-month-old *Gaa*$^{-/-}$ mice. These results show a reduced number of muscle spindles in *Gaa*$^{-/-}$ mice. They also suggest that the degenerative changes observed in 8.5-month-old *Gaa*$^{-/-}$ mice could lead to the loss of muscle spindles. The mean values for the number of muscle spindles in *Gaa*$^{-/-}$ and BL6 lines are given in Table 12 together with the corresponding standard deviations.

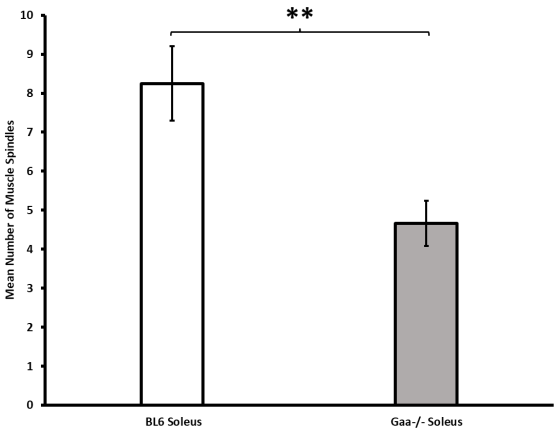

Figure 13. Mean Number of Muscle Spindles in the Soleus Muscle of the 8.5-month-old BL6 and *Gaa*$^{-/-}$ Mice. The soleus muscle of 8.5-month-old *Gaa*$^{-/-}$ mice had a significantly lower number of muscle spindles than the soleus muscle of 8.5-month-old BL6 mice. Mean ± Standard deviation; BL6: N=3 mice; *Gaa*$^{-/-}$: N=3 mice; Student's t- test, P-values: *<0.05, **<0.01, ***<0.001.

Table 12. Mean Values of the Number of Muscle Spindles and ± STDEV in Soleus Muscle of 8.5-month-old BL6 and *Gaa*$^{-/-}$ Mice.

Muscle Spindles in Soleus Muscle			
	Mean	± STDEV	P-Value
8.5-month-old BL6	8.25	0.96	0.002
8.5-month-old *Gaa*$^{-/-}$	4.67	0.58	

4.3.3 Quantitative Analysis of Sarcomeres

In order to investigate if the contractile part of muscle spindles is also affected by absence of GAA enzymatic activity, the number of sarcomeres per µm in the 2.5-month-old and 8.5-month-old wildtype and in *Gaa*$^{-/-}$ mice were counted. I observed no apparent statistical difference between the number of sarcomeres per µm in 2.5-month-old and 8.5-month-old wildtype and *Gaa*$^{-/-}$ mice for both, the soleus and the EDL muscle. These results show that the density of sarcomeres in the 2.5-month-old and 8.5-month-old *Gaa*$^{-/-}$ mice did not change compared to the age-matched control mice. The mean values for sarcomeres per µm in the *Gaa*$^{-/-}$ and BL6 lines are given in Table 13 together with the corresponding standard deviations.

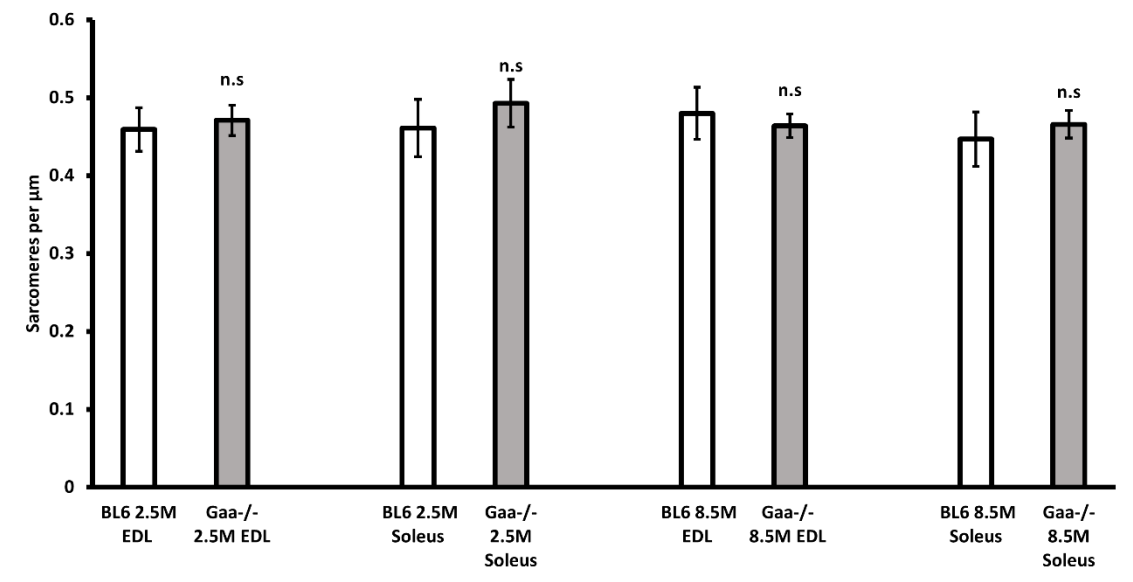

Figure 14. Number of Sarcomeres per µm in the EDL and Soleus Muscle in 2.5- and 8.5-month-old BL6 and *Gaa*$^{-/-}$ Mice. There was no significant difference in the number of sarcomeres per µm in the soleus and EDL muscle of 2.5-month-old and 8.5-month-old BL6 and *Gaa*$^{-/-}$ Mice. Mean ± Standard deviation; BL6: N=3 mice, n=9 spindles; *Gaa*$^{-/-}$: N=3 mice, n=9 spindles; Student's t- test, P-values: *<0.05, **<0.01, ***<0.001; M: month-old.

Table 13. Mean values (sarcomeres per µm) and ± STDEV in the EDL and Soleus Muscle in 2.5m-month-old and 8.5-month-old BL6 and *Gaa*$^{-/-}$ Mice.

Mean sarcomeres per µm						
	EDL Muscle			Soleus Muscle		
	Mean	± STDEV	P-Value	Mean	± STDEV	P-Value
2.5-month-old BL6 mice	0.459	0.028	0.384	0.461	0.037	0.071
2.5-month-old *Gaa*$^{-/-}$ mice	0.471	0.02		0.493	0.031	
8.5-month-old BL6 mice	0.48	0.034	0.336	0.447	0.035	0.319
8.5-month-old *Gaa*$^{-/-}$ mice	0.464	0.015		0.466	0.018	

5. Discussion

In my thesis, I qualitatively and quantitatively analyzed muscle spindles from mice with a genetic deficiency of the acid alpha-glucosidase enzyme. The lack of the GAA enzyme causes severe degeneration of extrafusal fibers in skeletal muscles and the nervous system, resulting in gait and posture instability in patients with Pompe disease, which increases the risk of falling and hospitalization (McIntosh et al., 2015; Valle et al., 2016; Lamartine S Monteiro & Remiche, 2019). Previous studies have shown that this instability can only be partly explained by the myopathy (Schneider et al., 2020). I therefore hypothesized that an altered proprioception causes these symptoms. Since muscle spindles are the main proprioceptors, I investigated if and how severely muscle spindles are affected in the GAA deficient mice. These mice have been used in numerous other studies regarding Pompe disease and have key features of both the infantile and adult forms of the disease (Bijvoet et al., 1998; Raben et al., 1998; Yi et al., 2017; Colella et al., 2019; Lee et al., 2020). Since the muscle wasting in Pompe disease is progressive, I analyzed 2.5-month-old and 8.5-month-old mice, to characterize the disease progression in muscle spindles. Furthermore, I investigated if muscle fiber composition plays a role in muscle spindle degeneration, since it is known that type 2 muscle fibers are more severely affected and more therapy-resistant in Pompe disease (Raben et al., 2007). To this end, I examined the predominantly slow twitch soleus muscle and predominantly fast twitch EDL muscle (Barclay et al., 1993; Soukup et al., 2002; Hettige et al., 2020). To explain the pathophysiology of Pompe disease, autophagy has emerged as one of the most important pathogenic processes. Since autophagic accumulation in extrafusal fibers has been demonstrated using the light chain 3-like protein (LC3A/B) antibody (Shea & Raben, 2009), I investigated if that might be also the case for the intrafusal fibers of the muscle spindle. In the following sections, I will discuss these issues separately.

5.1 Muscle Spindle Structural Changes

I started my investigation of the muscle spindle structure with a qualitative analysis. I first analyzed the morphological changes in muscle spindles of 2.5-month-old *Gaa*$^{-/-}$ mice and compared them to age-matched wildtype mice. The 2.5-month-old *Gaa*$^{-/-}$ mice had an intact muscle spindle structure similar to that of the age-matched control group. The muscle spindles had a normal distribution of nuclei, the morphology of the annulospiral endings was intact and the sensory nerve terminal had direct contact with the intrafusal fibers. Moreover, the contractile filaments were exclusively observed in the polar regions of the spindles. However, the quantitative analysis of these spindles showed there were already some minor changes present. The circumferential elements of the sensory nerve terminals had greater width and were shorter in length. One possible explanation for these structural changes could be glycogen deposits and/or autophagic buildup inside the circumferential elements. This is in accordance with the literature, where patients with Pompe disease have also been found to have glycogen deposits in their peripheral nervous system and dorsal root ganglia neurons (Gambetti et al., 1971; Falk et al., 2015; Lee et al., 2020). In contrast, the muscle spindles of the 8.5-month-old *Gaa*$^{-/-}$ mice had massive changes, especially in the morphology of the annulospiral endings, compared to the age-matched wildtype mice. The annulospiral endings were completely absent, had lost contact with the intrafusal fibers and had retracted and formed large varicosities. These varicosities are typical for the “dying back” mechanism, which refers to the progressive distal to proximal axonal degeneration that results from metabolic, toxic, or degenerative disorders (Benarroch, 2015). Muscle spindles from the gracile axonal dystrophy mouse line have shown similar alterations (Yong et al., 2021). In addition, in these muscle spindles the nuclei were not as clearly arranged in their typical chain or bag pattern. Since intrafusal fibers have a very distinct distribution of nuclei, the nuclear bag fibers with nuclei packed together in the equatorial region and the nuclear chain fibers with a single row of nuclei in the equatorial region, disarrangement of their nuclei might be a reflection of the degeneration of the intrafusal fiber.

The molecular mechanism that causes this degeneration is not clear. However, the exchange of signaling molecules between the intrafusal fiber and the sensory nerve terminal is required for the survival both cell types. One theory could be that the degeneration of the intrafusal fiber happens first, which subsequently leads to less secretion of neutrophin-3 - required for the survival of the sensory neuron (Ernfors et al., 1994; Klein et al., 1994) - causing degeneration and retraction of the sensory nerve. Another theory could be that the sensory nerve degenerates first because of the polyneuropathy which happens in Pompe patients (Sidman et al., 2008; Hobson-Webb et al., 2015; Lamartine S Monteiro & Remiche, 2019). This would lead to a reduced secretion of neuregulin-1 by the sensory neuron, which is required for the survival of intrafusal fibers (Hippenmeyer et al., 2002; Cheret et al., 2013). Lastly, it is also possible that the sensory neuron degeneration and intrafusal fiber degeneration are two separate processes that occur simultaneous.

A quantitative analysis of the circumferential elements in the 8.5-month-old *Gaa*$^{-/-}$ mice was not possible because of their total absence in these mice, indicating once again the severe degeneration which the annulospiral endings undergo in the 8.5-month-old *Gaa*$^{-/-}$ mice.

The contractile part of the muscle spindles was apparently not affected as much in regard to sarcomere density, compared to the degeneration of the annulospiral ending. There was no statistical difference between the number of sarcomeres per µm in 2.5-month-old and 8.5-month-old wildtype and *Gaa*$^{-/-}$ mice, indicating that the sarcomere density does not change with disease progression. Although in Pompe disease the type II extrafusal muscle fibers are preferentially affected, especially with respect to autophagic build-up (Raben et al., 2007), the degeneration of muscle spindles in the 8.5-month-old *Gaa*$^{-/-}$ mice occurred in both the predominantly slow twitch soleus muscles and predominantly fast twitch EDL muscle. This strongly suggests that the degeneration of muscle spindles happens independent of muscle fiber composition.

In conclusion, the data suggest that the muscle spindle degeneration in the 8.5-month-old *Gaa*$^{-/-}$ mice, could cause an altered proprioception, resulting in the gait

and posture instability with an increased risk for falling. This is in accordance with an autopsy study in a single Pompe patient which showed the intrafusal fibers of the muscle spindles have marked vacuolation and glycogen accumulation irrespective of the condition of their muscle of origin (van der Walt et al., 1987) and another study proving the gait and posture problems in Pompe patients (Schneider et al., 2020). Therefore, training that focuses on proprioceptive improvement might be a useful component in the therapy of Pompe patients. The differences in locomotion between quadrupedal mice and bipedal human must be taken into consideration, thus making a translation to humans difficult.

5.2 Autophagic Buildup Inside the Muscle Spindles

Autophagy (from Greek for “self-eating”) is a process, through which proteins and organelles are delivered to lysosomes for degradation and recycling. The main role of autophagy is to provide energy during phases of starvation. Under normal conditions autophagy serves as a quality control system by eliminating damaged organelles and proteins (Klionsky, 2007; Yim & Mizushima, 2020). The main pathogenic mechanism to explain Pompe disease has been accumulation of glycogen in lysosomes, resulting in enlargement and finally rupture of lysosomes. However, poor response of skeletal muscle to enzyme replacement therapy prompted a reassessment of disease mechanisms (Raben et al., 2012). Accumulation of autophagic debris in skeletal muscles from mice with Pompe disease, suggested autophagy as a potential pathogenic mechanism in Pompe disease. Especially since glycogen appears to enter lysosomes via autophagy (Raben et al., 2010). The discovery of the MAP1LC3 (microtubule - associated protein light chain 3) as a highly specific marker for autophagosomes, has made it possible to study autophagy on the cellular level. Since the autophagic process is disrupted in *Gaa*$^{-/-}$ mice and in Pompe disease patients and since there is an accumulation of autophagosomes in extrafusal fibers (Lim et al., 2014; Kohler et al., 2018), I investigated if there is any autophagic buildup also in the intrafusal fibers of the muscle spindle using the antibody against the LC3A/B protein. In both, the 2.5-

month-old and 8.5-month-old wildtype there was no autophagic build-up inside the muscle spindle. However, in the 2.5-month-old *Gaa*$^{-/-}$ mice I observed a small number of autophagic vacuoles inside the muscle spindle. In contrast, in the 8.5-month-old *Gaa*$^{-/-}$ mice there was considerable autophagic build-up inside the intrafusal fibers of the muscle spindle and in the vGluT1-postive varicosities. These results show that the muscle spindles are also affected by autophagy, and that the autophagic build-up inside the muscle spindles could contribute to their degeneration. Furthermore, it appears that a disruption of autophagy might begin in mice as early as 2.5-months of age in the *Gaa*$^{-/-}$ mice.

5.3 Number of Muscle Spindles in Wildtype and *Gaa*$^{-/-}$ Mice

To investigate if the degenerative processes induced by the absence of the GAA enzyme also affects the number of muscle spindles in skeletal muscle, I quantitatively analyzed the number of muscle spindles in the soleus muscles of 8.5-month-old *Gaa*$^{-/-}$ mice and compared this number to the age-matched wildtype mice. The muscle spindles were identified using indirect immunofluorescence and the epifluorescent microscope. Using two morphological criteria, the positive staining of the annulospiral endings with vGluT1 and the positive DAPI staining with the characteristic distribution of the nuclei within the intrafusal bag and chain fibers, it was possible to detect muscle spindles within serial sections of the soleus muscle. The data showed that the number of muscle spindles in the 8.5-month-old *Gaa*$^{-/-}$ mice was lower (4.67 in *Gaa*$^{-/-}$ mice compared to 8.25 in wildtype mice) than in the 8.5-month-old- wildtype mice with a statistical significance. This finding implies that the lower number of muscle spindles in *Gaa*$^{-/-}$ mice might affect proprioception. One caveat should, however, be noted: identifying muscle spindles in in sections from 8.5-month-old *Gaa*$^{-/-}$ mice was considerably difficult. Due to the lack of annulospiral endings in the muscle spindles of these mice, vGluT1 staining was not a reliable approach to detect the spindles. Similarly, because the intrafusal bag and chain fiber had lost their typical structure due to degeneration, the DAPI staining was less accurate. This might have affected the

quantification since it might lead to an underrepresentation of the number of muscle spindles per muscle. Another point to mention is that when compared to previous research, the number of muscle spindles detected in wildtype mice was on the lower end of the average (Gerwin et al., 2020).

6. References

Almodóvar-Payá, A., Villarreal-Salazar, M., de Luna, N., Nogales-Gadea, G., Real-Martínez, A., Andreu, A. L., Martín, M. A., Arenas, J., Lucia, A., Vissing, J., Krag, T., & Pinós, T. (2020). Preclinical Research in Glycogen Storage Diseases: A Comprehensive Review of Current Animal Models. *International Journal of Molecular Sciences*, *21*(24), E9621. https://doi.org/10.3390/ijms21249621

Ausems, M. G., Verbiest, J., Hermans, M. P., Kroos, M. A., Beemer, F. A., Wokke, J. H., Sandkuijl, L. A., Reuser, A. J., & van der Ploeg, A. T. (1999). Frequency of glycogen storage disease type II in The Netherlands: Implications for diagnosis and genetic counselling. *European Journal of Human Genetics: EJHG*, *7*(6), 713–716. https://doi.org/10.1038/sj.ejhg.5200367

Banks, R. W. (1986). Observations on the primary sensory ending of tenuissimus muscle spindles in the cat. *Cell and Tissue Research*, *246*(2), 309–319. https://doi.org/10.1007/BF00215893

Banks, R. W. (1994). The motor innervation of mammalian muscle spindles. *Progress in Neurobiology*, *43*(4–5), 323–362. https://doi.org/10.1016/0301-0082(94)90059-0

Banks, R. W. (2015). The innervation of the muscle spindle: A personal history. *Journal of Anatomy*, *227*(2), 115–135. https://doi.org/10.1111/joa.12297

Banks, R. W., Barker, D., Stacey, M. J., & Young, J. Z. (1982). Form and distribution of sensory terminals in cat hindlimb muscle spindles. *Philosophical Transactions of the Royal Society of London. B, Biological Sciences*, *299*(1096), 329–364. https://doi.org/10.1098/rstb.1982.0136

Banks, R. W., Harker, D. W., & Stacey, M. J. (1977). A study of mammalian intrafusal muscle fibres using a combined histochemical and ultrastructural technique. *Journal of Anatomy*, *123*(Pt 3), 783–796.

Barclay, C. J., Constable, J. K., & Gibbs, C. L. (1993). Energetics of fast- and slow-twitch muscles of the mouse. *The Journal of Physiology*, *472*(1), 61–80. https://doi.org/10.1113/jphysiol.1993.sp019937

Barker, D. (1948). The Innervation of the Muscle-Spindle. *Journal of Cell Science*, *s3-89*(6), 143–185. https://doi.org/10.1242/jcs.s3-89.6.143

Benarroch, E. E. (2015). Acquired axonal degeneration and regeneration: Recent insights and clinical correlations. *Neurology*, *84*(20), 2076–2085. https://doi.org/10.1212/WNL.0000000000001601

Bijvoet, A. G., van de Kamp, E. H., Kroos, M. A., Ding, J. H., Yang, B. Z., Visser, P., Bakker, C. E., Verbeet, M. P., Oostra, B. A., Reuser, A. J., & van der Ploeg, A. T. (1998). Generalized glycogen storage and cardiomegaly in a knockout mouse model of Pompe disease. *Human Molecular Genetics*, *7*(1), 53–62. https://doi.org/10.1093/hmg/7.1.53

Bischoff, G. (1932). Zum klinischen Bild der Glykogen-Speicherungskrankheit (Glykogenose). *Zeitschrift für Kinderheilkunde*, *52*(6), 722–726. https://doi.org/10.1007/BF02248461

Blecher, R., Krief, S., Galili, T., Assaraf, E., Stern, T., Anekstein, Y., Agar, G., & Zelzer, E. (2017). The Proprioceptive System Regulates Morphologic Restoration of Fractured Bones. *Cell Reports*, *20*(8), 1775–1783. https://doi.org/10.1016/j.celrep.2017.07.073

Blecher, R., Krief, S., Galili, T., Biton, I. E., Stern, T., Assaraf, E., Levanon, D., Appel, E., Anekstein, Y., Agar, G., Groner, Y., & Zelzer, E. (2017). The Proprioceptive System Masterminds Spinal Alignment: Insight into the Mechanism of Scoliosis. *Developmental Cell*, *42*(4), 388-399.e3. https://doi.org/10.1016/j.devcel.2017.07.022

Boyd, I. A., Gladden, M. H., McWilliam, P. N., & Ward, J. (1977). Control of dynamic and static nuclear bag fibres and nuclear chain fibres by gamma and beta axons in isolated cat muscle spindels. *The Journal of Physiology*, *265*(1), 133–162.

Cheret, C., Willem, M., Fricker, F. R., Wende, H., Wulf-Goldenberg, A., Tahirovic, S., Nave, K.-A., Saftig, P., Haass, C., Garratt, A. N., Bennett, D. L., & Birchmeier, C. (2013). Bace1 and Neuregulin-1 cooperate to control formation and maintenance of muscle spindles. *The EMBO Journal*, *32*(14), 2015–2028. https://doi.org/10.1038/emboj.2013.146

Colella, P., Sellier, P., Costa Verdera, H., Puzzo, F., van Wittenberghe, L., Guerchet, N., Daniele, N., Gjata, B., Marmier, S., Charles, S., Simon Sola, M., Ragone, I., Leborgne, C., Collaud, F., & Mingozzi, F. (2019). AAV Gene Transfer with Tandem Promoter Design Prevents Anti-transgene Immunity and Provides Persistent Efficacy in Neonate Pompe Mice. *Molecular Therapy - Methods & Clinical Development*, *12*, 85–101. https://doi.org/10.1016/j.omtm.2018.11.002

Dasouki, M., Jawdat, O., Almadhoun, O., Pasnoor, M., McVey, A. L., Abuzinadah, A., Herbelin, L., Barohn, R. J., & Dimachkie, M. M. (2014). Pompe Disease: Literature Review and Case Series. *Neurologic Clinics*, *32*(3), 751–ix. https://doi.org/10.1016/j.ncl.2014.04.010

De-Doncker, L., Picquet, F., Browne, G. B., & Falempin, M. (2002). Expression of Myosin Heavy Chain Isoforms Along Intrafusal Fibers of Rat Soleus Muscle Spindles After 14 Days of Hindlimb Unloading. *Journal of Histochemistry & Cytochemistry*, *50*(11), 1543–1553. https://doi.org/10.1177/002215540205001115

De-Doncker, L., Picquet, F., Petit, J., & Falempin, M. (2003). Characterization of Spindle Afferents in Rat Soleus Muscle Using Ramp-and-Hold and Sinusoidal Stretches. *Journal of Neurophysiology*, *89*(1), 442–449. https://doi.org/10.1152/jn.00153.2002

Dietz, V. (2002). Proprioception and locomotor disorders. *Nature Reviews Neuroscience*, *3*(10), Article 10. https://doi.org/10.1038/nrn939

Eliceiri, K. W., Berthold, M. R., Goldberg, I. G., Ibáñez, L., Manjunath, B. S., Martone, M. E., Murphy, R. F., Peng, H., Plant, A. L., Roysam, B., Stuurman, N., Swedlow, J. R., Tomancak, P., & Carpenter, A. E. (2012). Biological imaging software tools. *Nature Methods*, *9*(7), Article 7. https://doi.org/10.1038/nmeth.2084

Ernfors, P., Lee, K.-F., Kucera, J., & Jaenisch, R. (1994). Lack of neurotrophin-3 leads to deficiencies in the peripheral nervous system and loss of limb proprioceptive afferents. *Cell*, *77*(4), 503–512. https://doi.org/10.1016/0092-8674(94)90213-5

Falk, D. J., Todd, A. G., Lee, S., Soustek, M. S., ElMallah, M. K., Fuller, D. D., Notterpek, L., & Byrne, B. J. (2015). Peripheral nerve and neuromuscular junction pathology in Pompe disease. *Human Molecular Genetics*, *24*(3), 625–636. https://doi.org/10.1093/hmg/ddu476

Gambetti, P., Dimauro, S., & Baker, L. (1971). Nervous System in Pompe's Disease: Ultrastructure and Biochemistry*†. *Journal of Neuropathology & Experimental Neurology*, *30*(3), 412–430. https://doi.org/10.1097/00005072-197107000-00008

Gerwin, L., Haupt, C., Wilkinson, K. A., & Kröger, S. (2019). Acetylcholine receptors in the equatorial region of intrafusal muscle fibres modulate mouse muscle spindle sensitivity. *The Journal of Physiology*, *597*(7), 1993–2006. https://doi.org/10.1113/JP277139

Gerwin, L., Rossmanith, S., Haupt, C., Schultheiß, J., Brinkmeier, H., Bittner, R. E., & Kröger, S. (2020). Impaired muscle spindle function in murine models of muscular dystrophy. *The Journal of Physiology*, *598*(8), 1591–1609. https://doi.org/10.1113/JP278563

Grimstone, S. K., & Hodges, P. W. (2003). Impaired postural compensation for respiration in people with recurrent low back pain. *Experimental Brain Research*, *151*(2), 218–224. https://doi.org/10.1007/s00221-003-1433-5

Hers, H. G. (1963). Alpha-Glucosidase deficiency in generalized glycogenstorage disease (Pompe's disease). *The Biochemical Journal*, *86*, 11–16. https://doi.org/10.1042/bj0860011

Hettige, P., Tahir, U., Nishikawa, K. C., & Gage, M. J. (2020). Comparative analysis of the transcriptomes of EDL, psoas, and soleus muscles from mice. *BMC Genomics*, *21*(1), 808. https://doi.org/10.1186/s12864-020-07225-2

Hippenmeyer, S., Shneider, N. A., Birchmeier, C., Burden, S. J., Jessell, T. M., & Arber, S. (2002). A Role for Neuregulin1 Signaling in Muscle Spindle Differentiation. *Neuron*, *36*(6), 1035–1049. https://doi.org/10.1016/S0896-6273(02)01101-7

Hobson-Webb, L. D., Austin, S. L., Jain, S., Case, L. E., Greene, K., & Kishnani, P. S. (2015). Small-Fiber Neuropathy in Pompe Disease: First Reported Cases and Prospective Screening of

a Clinic Cohort. *The American Journal of Case Reports*, *16*, 196–201. https://doi.org/10.12659/AJCR.893309

Honda, C. N. (1995). Differential distribution of calbindin-D28k and parvalbumin in somatic and visceral sensory neurons. *Neuroscience*, *68*(3), 883–892. https://doi.org/10.1016/0306-4522(95)00180-q

Horlings, C. G. C., Küng, U. M., van Engelen, B. G. M., Voermans, N. C., Hengstman, G. J. D., van der Kooi, A. J., Bloem, B. R., & Allum, J. H. J. (2009). Balance control in patients with distal versus proximal muscle weakness. *Neuroscience*, *164*(4), 1876–1886. https://doi.org/10.1016/j.neuroscience.2009.09.063

Kabeya, Y., Mizushima, N., Ueno, T., Yamamoto, A., Kirisako, T., Noda, T., Kominami, E., Ohsumi, Y., & Yoshimori, T. (2000). LC3, a mammalian homologue of yeast Apg8p, is localized in autophagosome membranes after processing. *The EMBO Journal*, *19*(21), 5720–5728. https://doi.org/10.1093/emboj/19.21.5720

Kiehn, O. (2016). Decoding the organization of spinal circuits that control locomotion. *Nature Reviews Neuroscience*, *17*(4), 224–238. https://doi.org/10.1038/nrn.2016.9

Kishnani, P. S., Amartino, H. M., Lindberg, C., Miller, T. M., Wilson, A., Keutzer, J., & Pompe Registry Boards of Advisors. (2013). Timing of diagnosis of patients with Pompe disease: Data from the Pompe registry. *American Journal of Medical Genetics. Part A*, *161A*(10), 2431–2443. https://doi.org/10.1002/ajmg.a.36110

Kishnani, P. S., Hwu, W.-L., Mandel, H., Nicolino, M., Yong, F., & Corzo, D. (2006). A retrospective, multinational, multicenter study on the natural history of infantile-onset Pompe disease. *The Journal of Pediatrics*, *148*(5), 671-676.e2. https://doi.org/10.1016/j.jpeds.2005.11.033

Kishnani, P. S., Steiner, R. D., Bali, D., Berger, K., Byrne, B. J., Case, L. E., Crowley, J. F., Downs, S., Howell, R. R., Kravitz, R. M., Mackey, J., Marsden, D., Martins, A. M., Millington, D. S., Nicolino, M., O'grady, G., Patterson, M. C., Rapoport, D. M., Slonim, A., … Watson, M. S. (2006). Pompe disease diagnosis and management guideline. *Genetics in Medicine*, *8*(5), 267–288. https://doi.org/10.1097/01.gim.0000218152.87434.f3

Klein, R., Silos-Santiago, I., Smeyne, R. J., Lira, S. A., Brambilla, R., Bryant, S., Zhang, L., Snider, W. D., & Barbacid, M. (1994). Disruption of the neurotrophin-3 receptor gene trkC eliminates la muscle afferents and results in abnormal movements. *Nature*, *368*(6468), Article 6468. https://doi.org/10.1038/368249a0

Klionsky, D. J. (2007). Autophagy: From phenomenology to molecular understanding in less than a decade. *Nature Reviews Molecular Cell Biology*, *8*(11), 931–937. https://doi.org/10.1038/nrm2245

Kohler, L., Puertollano, R., & Raben, N. (2018). Pompe Disease: From Basic Science to Therapy. *Neurotherapeutics*, *15*(4), 928–942. https://doi.org/10.1007/s13311-018-0655-y

Kröger, S. (2018). Proprioception 2.0: Novel functions for muscle spindles. *Current Opinion in Neurology*, *31*(5), 592–598. https://doi.org/10.1097/WCO.0000000000000590

Kröger, S., & Watkins, B. (2021). Muscle spindle function in healthy and diseased muscle. *Skeletal Muscle*, *11*(1), 3. https://doi.org/10.1186/s13395-020-00258-x

Kucera, J., & Walro, J. M. (1995). An immunocytochemical marker for early type I muscle fibers in the developing rat hindlimb. *Anatomy and Embryology*, *192*(2), 137–147. https://doi.org/10.1007/BF00186002

Kucera, J., Walro, J. M., & Gorza, L. (1992). Expression of type-specific MHC isoforms in rat intrafusal muscle fibers. *The Journal of Histochemistry and Cytochemistry: Official Journal of the Histochemistry Society*, *40*(2), 293–307. https://doi.org/10.1177/40.2.1552171

Lamartine S Monteiro, M., & Remiche, G. (2019). Late-onset Pompe disease associated with polyneuropathy. *Neuromuscular Disorders: NMD*, *29*(12), 968–972. https://doi.org/10.1016/j.nmd.2019.08.016

Lee, N.-C., Peng, W.-H., Tsai, L.-K., Lu, Y.-H., Wang, H.-C., Shih, Y.-C., Pung, Z.-X., Hu, H.-Y., Hwu, W.-L., Tseng, W.-Y. I., & Chien, Y.-H. (2020). Ultrastructural and diffusion tensor imaging studies reveal axon abnormalities in Pompe disease mice. *Scientific Reports*, *10*(1), Article 1. https://doi.org/10.1038/s41598-020-77193-w

Lieberman, A. P., Puertollano, R., Raben, N., Slaugenhaupt, S., Walkley, S. U., & Ballabio, A. (2012). Autophagy in lysosomal storage disorders. *Autophagy*, *8*(5), 719–730. https://doi.org/10.4161/auto.19469

Lim, J.-A., Li, L., & Raben, N. (2014). Pompe disease: From pathophysiology to therapy and back again. *Frontiers in Aging Neuroscience*, *6*. https://www.frontiersin.org/article/10.3389/fnagi.2014.00177

Lionikas, A., Smith, C. J., Smith, T. L., Bünger, L., Banks, R. W., & Bewick, G. S. (2013). Analyses of muscle spindles in the soleus of six inbred mouse strains. *Journal of Anatomy*, *223*(3), 289–296. https://doi.org/10.1111/joa.12076

Manuel, M., & Zytnicki, D. (2011). Alpha, beta and gamma motoneurons: Functional diversity in the motor system's final pathway. *Journal of Integrative Neuroscience*, *10*(03), 243–276. https://doi.org/10.1142/S0219635211002786

Martiniuk, F., Bodkin, M., Tzall, S., & Hirschhorn, R. (1991). Isolation and Partial Characterization of the Structural Gene for Human Acid Alpha Glucosidase. *DNA and Cell Biology*, *10*(4), 283–292. https://doi.org/10.1089/dna.1991.10.283

Matthews, P. B. C. (1974). Mammalian Muscle Receptors and their Central Actions. *American Journal of Physical Medicine & Rehabilitation*, *53*(3), 143–144.

Matthews, P. B. C. (2015). Where Anatomy led, Physiology followed: A survey of our developing understanding of the muscle spindle, what it does and how it works. *Journal of Anatomy*, *227*(2), 104–114. https://doi.org/10.1111/joa.12345

McIntosh, P. T., Case, L. E., Chan, J. M., Austin, S. L., & Kishnani, P. (2015). Characterization of gait in late onset Pompe disease. *Molecular Genetics and Metabolism*, *116*(3), 152–156. https://doi.org/10.1016/j.ymgme.2015.09.001

Mears, S. C., & Frank, E. (1997). Formation of Specific Monosynaptic Connections between Muscle Spindle Afferents and Motoneurons in the Mouse. *Journal of Neuroscience*, *17*(9), 3128–3135. https://doi.org/10.1523/JNEUROSCI.17-09-03128.1997

Miller, J. B., Crow, M. T., & Stockdale, F. E. (1985). Slow and fast myosin heavy chain content defines three types of myotubes in early muscle cell cultures. *Journal of Cell Biology*, *101*(5), 1643–1650. https://doi.org/10.1083/jcb.101.5.1643

Mizushima, N. (2007). Autophagy: Process and function. *Genes & Development*, *21*(22), 2861–2873. https://doi.org/10.1101/gad.1599207

Musumeci, O., Marino, S., Granata, F., Morabito, R., Bonanno, L., Brizzi, T., Lo Buono, V., Corallo, F., Longo, M., & Toscano, A. (2019). Central nervous system involvement in late-onset Pompe disease: Clues from neuroimaging and neuropsychological analysis. *European Journal of Neurology*, *26*(3), 442-e35. https://doi.org/10.1111/ene.13835

Niño, M. Y., Wijgerde, M., de Faria, D. O. S., Hoogeveen-Westerveld, M., Bergsma, A. J., Broeders, M., van der Beek, N. A. M. E., van den Hout, H. J. M., van der Ploeg, A. T., Verheijen, F. W., & Pijnappel, W. W. M. P. (2021). Enzymatic diagnosis of Pompe disease: Lessons from 28 years of experience. *European Journal of Human Genetics: EJHG*, *29*(3), 434–446. https://doi.org/10.1038/s41431-020-00752-2

Oliver, K. M., Florez-Paz, D. M., Badea, T. C., Mentis, G. Z., Menon, V., & Nooij, J. C. de. (2020). *Molecular development of muscle spindle and Golgi tendon organ sensory afferents revealed by single proprioceptor transcriptome analysis* (p. 2020.04.03.023986). bioRxiv. https://doi.org/10.1101/2020.04.03.023986

Pedrosa, F., Soukup, T., & Thornell, L.-E. (1990). Expression of an alpha cardiac-like myosin heavy chain in muscle spindle fibres. *Histochemistry*, *95*(2), 105–113. https://doi.org/10.1007/BF00266582

Peruzzo, P., Pavan, E., & Dardis, A. (2019). Molecular genetics of Pompe disease: A comprehensive overview. *Annals of Translational Medicine*, *7*(13), 278. https://doi.org/10.21037/atm.2019.04.13

Pompe, JC. (1932). Over idiopathische hypertrophie van het hart. *Ned Tijdschr Geneeskd*, *76*, 304–311.

Proske, U. (1997). The Mammalian Muscle Spindle. *Physiology*, *12*(1), 37–42. https://doi.org/10.1152/physiologyonline.1997.12.1.37

Proske, U., & Gandevia, S. C. (2012). The proprioceptive senses: Their roles in signaling body shape, body position and movement, and muscle force. *Physiological Reviews*, *92*(4), 1651–1697. https://doi.org/10.1152/physrev.00048.2011

Putschar, M. (1932). Uber angeborene Glykogenspeicher-Krankheit des herzens. *Beitr. Pathol. Anat. Allg. Pathol*, *90*, 222.

Raben, N., Nagaraju, K., Lee, E., Kessler, P., Byrne, B., Lee, L., LaMarca, M., King, C., Ward, J., Sauer, B., & Plotz, P. (1998). Targeted disruption of the acid alpha-glucosidase gene in mice causes an illness with critical features of both infantile and adult human glycogen storage disease type II. *The Journal of Biological Chemistry*, *273*(30), 19086–19092. https://doi.org/10.1074/jbc.273.30.19086

Raben, N., Nagaraju, K., Lee, E., & Plotz, P. (2000). Modulation of disease severity in mice with targeted disruption of the acid alpha-glucosidase gene. *Neuromuscular Disorders*, *10*(4–5), 283–291. https://doi.org/10.1016/s0960-8966(99)00117-0

Raben, N., Schreiner, C., Baum, R., Takikita, S., Xu, S., Xie, T., Myerowitz, R., Komatsu, M., Van Der Meulen, J. H., Nagaraju, K., Ralston, E., & Plotz, P. H. (2010). Suppression of autophagy permits successful enzyme replacement therapy in a lysosomal storage disorder—Murine Pompe disease. *Autophagy*, *6*(8), 1078–1089. https://doi.org/10.4161/auto.6.8.13378

Raben, N., Takikita, S., Pittis, M. G., Bembi, B., Marie, S. K. N., Roberts, A., Page, L., Kishnani, P. S., Schoser, B. G. H., Chien, Y.-H., Ralston, E., Nagaraju, K., & Plotz, P. H. (2007). Deconstructing Pompe Disease by Analyzing Single Muscle Fibers: “To See a World in a Grain of Sand….” *Autophagy*, *3*(6), 546–552. https://doi.org/10.4161/auto.4591

Raben, N., Wong, A., Ralston, E., & Myerowitz, R. (2012). Autophagy and mitochondria in Pompe disease: Nothing is so new as what has long been forgotten. *American Journal of Medical Genetics Part C: Seminars in Medical Genetics*, *160C*(1), 13–21. https://doi.org/10.1002/ajmg.c.31317

Ruffini, A. (1898). On the Minute Anatomy of the Neuromuscular Spindles of the Cat, and on their Physiological Significance. *The Journal of Physiology*, *23*(3), 190-208.3.

Schindelin, J., Arganda-Carreras, I., Frise, E., Kaynig, V., Longair, M., Pietzsch, T., Preibisch, S., Rueden, C., Saalfeld, S., Schmid, B., Tinevez, J.-Y., White, D. J., Hartenstein, V., Eliceiri, K., Tomancak, P., & Cardona, A. (2012). Fiji: An open-source platform for biological-image analysis. *Nature Methods*, *9*(7), Article 7. https://doi.org/10.1038/nmeth.2019

Schneider, I., Zierz, S., Schulze, S., Delank, K.-S., Laudner, K. G., Brill, R., & Schwesig, R. (2020). Characterization of Gait and Postural Regulation in Late-Onset Pompe Disease. *Applied Sciences*, *10*(19), Article 19. https://doi.org/10.3390/app10197001

Schoser, B. (2019). Pompe disease: What are we missing? *Annals of Translational Medicine*, *7*(13), 292. https://doi.org/10.21037/atm.2019.05.29

Schröder, J. M., Bodden, H., Hamacher, A., & Verres, C. (1989). Scanning electron microscopy of teased intrafusal muscle fibers from rat muscle spindles. *Muscle & Nerve*, *12*(3), 221–232. https://doi.org/10.1002/mus.880120311

Shea, L., & Raben, N. (2009). Autophagy in skeletal muscle: Implications for Pompe disease. *International Journal of Clinical Pharmacology and Therapeutics*, *47*(Suppl 1), S42–S47.

Sherrington, C. S. (1907). ON THE PROPRIO-CEPTIVE SYSTEM, ESPECIALLY IN ITS RE-FLEX ASPECT. *Brain*, *29*(4), 467–482. https://doi.org/10.1093/brain/29.4.467

Sidman, R. L., Taksir, T., Fidler, J., Zhao, M., Dodge, J. C., Passini, M. A., Raben, N., Thurberg, B. L., Cheng, S. H., & Shihabuddin, L. S. (2008). Temporal Neuropathological and Behavioral Phenotype of 6Neo/6Neo Pompe Disease Mice. *Journal of Neuropathology and Experimental Neurology*, *67*(8), 803–818. https://doi.org/10.1097/NEN.0b013e3181815994

Soukup, T., Zacharová, G., & Smerdu, V. (2002). Fibre type composition of soleus and extensor digitorum longus muscles in normal female inbred Lewis rats. *Acta Histochemica*, *104*(4), 399–405. https://doi.org/10.1078/0065-1281-00660

Toscano, A., Rodolico, C., & Musumeci, O. (2019). Multisystem late onset Pompe disease (LOPD): An update on clinical aspects. *Annals of Translational Medicine*, *7*(13), 10–10. https://doi.org/10.21037/atm.2019.07.24

Toscano, A., & Schoser, B. (2013). Enzyme replacement therapy in late-onset Pompe disease: A systematic literature review. *Journal of Neurology*, *260*(4), 951–959. https://doi.org/10.1007/s00415-012-6636-x

Tsai, L.-K., Hwu, W.-L., Lee, N.-C., Huang, P.-H., & Chien, Y.-H. (2019). Clinical features of Pompe disease with motor neuronopathy. *Neuromuscular Disorders*, *29*(11), 903–906. https://doi.org/10.1016/j.nmd.2019.09.011

Valle, M. S., Casabona, A., Fiumara, A., Castiglione, D., Sorge, G., & Cioni, M. (2016). Quantitative analysis of upright standing in adults with late-onset Pompe disease. *Scientific Reports*, *6*(1), Article 1. https://doi.org/10.1038/srep37040

van der Walt, J. D., Swash, M., Leake, J., & Cox, E. L. (1987). The pattern of involvement of adult-onset acid maltase deficiency at autopsy. *Muscle & Nerve*, *10*(3), 272–281. https://doi.org/10.1002/mus.880100311

Walro, J. M., & Kucera, J. (1999). Why adult mammalian intrafusal and extrafusal fibers contain different myosin heavy-chain isoforms. *Trends in Neurosciences*, *22*(4), 180–184. https://doi.org/10.1016/s0166-2236(98)01339-3

Wang, Z., Li, L., & Frank, E. (2012). The role of muscle spindles in the development of the monosynaptic stretch reflex. *Journal of Neurophysiology*, *108*(1), 83–90. https://doi.org/10.1152/jn.00074.2012

Watkins, B., Schuster, H. M., Gerwin, L., Schoser, B., & Kröger, S. (2022). The effect of methocarbamol and mexiletine on murine muscle spindle function. *Muscle & Nerve*, *n/a*(n/a). https://doi.org/10.1002/mus.27546

Wu, S.-X., Koshimizu, Y., Feng, Y.-P., Okamoto, K., Fujiyama, F., Hioki, H., Li, Y.-Q., Kaneko, T., & Mizuno, N. (2004). Vesicular glutamate transporter immunoreactivity in the central and peripheral endings of muscle-spindle afferents. *Brain Research*, *1011*(2), 247–251. https://doi.org/10.1016/j.brainres.2004.03.047

Yi, H., Sun, T., Armstrong, D., Borneman, S., Yang, C., Austin, S., Kishnani, P. S., & Sun, B. (2017). Antibody-mediated enzyme replacement therapy targeting both lysosomal and cytoplasmic glycogen in Pompe disease. *Journal of Molecular Medicine*, *95*(5), 513–521. https://doi.org/10.1007/s00109-017-1505-9

Yim, W. W.-Y., & Mizushima, N. (2020). Lysosome biology in autophagy. *Cell Discovery*, *6*(1), Article 1. https://doi.org/10.1038/s41421-020-0141-7

Yong, Y., Hunter-Chang, S., Stepanova, E., & Deppmann, C. (2021). Axonal spheroids in neurodegeneration. *Molecular and Cellular Neuroscience*, *117*, 103679. https://doi.org/10.1016/j.mcn.2021.103679

Young, S. P., Piraud, M., Goldstein, J. L., Zhang, H., Rehder, C., Laforet, P., Kishnani, P. S., Millington, D. S., Bashir, M. R., & Bali, D. S. (2012). Assessing disease severity in Pompe disease: The roles of a urinary glucose tetrasaccharide biomarker and imaging techniques. *American Journal of Medical Genetics Part C: Seminars in Medical Genetics*, *160C*(1), 50–58. https://doi.org/10.1002/ajmg.c.31320

Zhang. (2014). *Formation of cholinergic synapse-like specializations at developing murine muscle spindles | Elsevier Enhanced Reader*. https://doi.org/10.1016/j.ydbio.2014.07.011

7. Appendix

7.1 List of abbreviations

BL6 mice	C57BL/6J
BSA	Bovine serum albumin
CE	Circumferential elements
CK	Creatine kinase
CMA	Chaperone-mediated autophagy
DAPI	4′,6-diamidino-2-phenylindole
DRG	Dorsal root ganglion
EDL	Extensor digitorum longus
ERT	Enzyme replacement therapy
Gaa$^{-/-}$ mice	B6;129-*Gaa*^{tm1Rabn}/J
IHC	Immunohistochemistry
IOPD	Infantile-onset Pompe disease
LOPD	Late-onset Pompe disease
MRI	Magnetic resonance imaging
$Na_v1.4$	Voltage gated sodium channel 1.4
PBS	Phosphate buffered saline
PBS-T	Phosphate buffered saline with Tween
PFA	Paraformaldehyde
vGluT1	Vesicular glutamate transporter 1

7.2 List of figures

7.3 List of tables

8. Acknowledgements

I would first like to express my sincere gratitude to my supervisor, Prof. Dr. Stephan Kröger, for giving me the opportunity to undertake this fascinating project in his laboratory. I am deeply thankful for his outstanding supervision, guidance, and constant support throughout the project, as well as his assistance in securing funding.

I would also like to thank all of the members of the lab group of Prof. Kröger, including Arlind Lamcaj, Bridgette Watkins, Dr.Corinna Haupt and especially Jürgen Schultheiß for their assistance with immunohistochemistry and confocal microscopy.

I am also grateful to the German Academic Exchange Service (DAAD) for providing me with a scholarship during this project.

Lastly, I want to thank my family and friends for their unwavering support and encouragement during this journey. Without their belief in me, I would not have made it this far.

Affidavit

Affidavit

Rafuna, Andi

Surname, first name

Großhaderner Straße 9

Street

82152, Planegg, Germany

Zip code, town, country

I hereby declare that the submitted thesis entitled:

Muscle Spindle Structure in a Mouse Model for Pompe Disease

……

is my own work. I have only used the sources indicated and have not made unauthorized use of services of a third party. Where the work of others has been quoted or reproduced, the source is always given.

I further declare that the submitted thesis or parts thereof have not been presented as part of an examination degree to any other university.

Munich, 18.02.2025 — Andi Rafuna

place, date — Signature doctoral candidate

Parts of this thesis have been published:
Watkins, B., Schultheiß, J., Rafuna, A., Hintze, S., Meinke, P., Schoser, B., & Kröger, S. (2023). Degeneration of muscle spindles in a murine model of Pompe disease. Sci Rep, 13(1), 6555.

Confirmation of Congruency

LMU LUDWIG-MAXIMILIANS-UNIVERSITÄT MÜNCHEN | Promotionsbüro Medizinische Fakultät | MMRS

Confirmation of congruency between printed and electronic version of the doctoral thesis

Rafuna, Andi

Surname, first name

Großhaderner Straße 9

Street

82152, Planegg, Germany

Zip code, town, country

I hereby declare that the submitted thesis entitled:

Muscle Spindle Structure in a Mouse Model for Pompe Disease

……

is congruent with the printed version both in content and format.

Munich, 18.02.2025

place, date

Andi Rafuna

Signature doctoral candidate

List of publications

Watkins, B., Schultheiß, J., Rafuna, A., Hintze, S., Meinke, P., Schoser, B., & Kröger, S. (2023). Degeneration of muscle spindles in a murine model of Pompe disease. Sci Rep, 13(1), 6555.